The Effect of Galanin alone and Combined with Estrogen in a Cuprizone-induced Demyelination Mouse Model of Multiple Sclerosis

By

Lin Zhang

A Thesis submitted to the Faculty of Graduate Studies of The University of Manitoba in partial fulfilment of the requirements of the degree of

MASTER OF SCIENCE

Department of Human Anatomy and Cell Science

University of Manitoba

Winnipeg

Abstract

Multiple Sclerosis (MS) is an autoimmune demyelination disease of the central nervous system (CNS). To date, there is no cure for MS. The traditional immunotherapies so far have not been able to stop the progression of the disease. Consequently, a new strategy of neuroprotection has been seriously considered as a candidate for the next generation of treatment.

Galanin (GAL) is an inducible bioactive neuropeptide, widely distributed in the nervous system. It has diverse regulatory effects in the nervous system including neuroprotection. The expression of galanin is induced by the administration of estrogen and is increased during pregnancy in rodents. In women with MS, pregnancy has a protective effect associated with significant remission of MS symptoms during the second and third trimester.

In this study, using the cuprizone (CPZ) demyelination model of MS I demonstrated that GAL has a pronounced neuroprotective effect on demyelination and remyelination, with estrogen the protection was further enhanced. Moreover, I also found differential activation of GAL receptors in the demyelination and remyelination processes.

These results suggest GAL alone or combined with estrogen might introduce next generation strategies for the treatment of MS.

Acknowledgments

This thesis would not have been possible without the kind support and enduring love of my sweet wife Yu (Sophie) Wu, my dear mom Shu-lan Li and dad Shi-xue Zhang.

There are many people I would like to thank for their help and guidance over the last three years study. Above all, it is an honor for me to present sincere thanks to my supervisors Dr. Maria E. Vrontakis and Dr. Ji-ming Kong for their novel advice, strong support and warm-hearted care. My thanks then go to the other members of my committee: Dr. Hugo Bergen, Dr. Fiona Parkinson and Dr. Emma Frost for their valuable suggestions and for their patience throughout the entire graduate program.

I greatly appreciate the help from the other members of our department, especially from the Head of our Department Dr. Thomas Klonisch, Dr. Jerry Vriend and Dr. Xin-min Li.

I wish to thank Dr. James Thliveris for the great technical support for electron microscopy and the wonderful training. A big thank you to Ingo Schroedter M.L.T. , a senior technologist in the Department of Hematopathology in HSC who trained me how to safely handle RNA samples, and how to face the failures in experiment. And thank you to Paul Perumal, our former departmental technician, his rich experimental experience and the helpful practical advice helped me in learning a reliable basic histological skill.

During the last three years I have made many sweet friends. They not only encouraged and helped me in the lab, but also greatly enriched my Canadian life in past few years.

Thank you to my friends: Adrian, Conny, Cheng-ren, Handi, Hong (Helena), Jacqueline, Jie-qun, Leilanie, Nicole, Ruo-yang, Sheng-hua, Teng and Xue-ping.

Lastly, my deepest gratitude goes to all of my warm family. My cousin Yu-Song (Alvin) Zhang, who taught me to be strong and cheered up me during hard times. My aunt Jin-rong Li, Cheng-rong Zhou and my uncle Chun-mu Li and Chang-lin Zhu, who always cares about my health and happiness. And a big thank you to my cousin Guo Zhu and Xin Li and their family for taking care of my parents when I were away from home.

I would like to dedicate this thesis to my mom, Mrs. Shu-lan Li. There is no doubt in my mind that without her pure love I could not have completed this process. 本文谨献于我的母亲李书兰女士。

Table of Contents

List of Figures

List of Tables

Abbreviations

12wCPZ	twelve-week cuprizone (challenge)
12wCPZ+3wR	twelve-week cuprizone (challenge) plus three-week recovery
6wCPZ	six-week cuprizone (challenge)
6wCPZ+3wR	six-week cuprizone (challenge) plus three-week recovery
aco	anterior commissure/olfactory limb
ANOVA	analysis of variance
BBB	blood brain barrier
CC	corpus callosum
cing	cingulum bundle
CNS	central nervous system
CP	caudoputamen
CPZ	cuprizone
CTL	control
DAB	diaminobenzidine
DRG	dorsal root ganglia
EAE	experimental autoimmune encephalomyelitis
ec	external capsule
EM	electron microscopy
ER	estrogen receptor
E1	estrone
E2	estradiol
E3	estriol

GAL	galanin
GALP	galanin-like peptide
GalR1	galanin receptor subtype 1
GalR2	galanin receptor subtype 2
GalR3	galanin receptor subtype 3
GalRs	galanin receptors
GAPDH	glyceraldehyde-3-phosphate dehydrogenase
GFAP	glial fibrillary acidic protein
GH	growth hormone
GMAP	galanin message-associated peptide
GST-π	glutathione s-transferase π form
Hypo,HY	hypothalamus
IHC	immunohistochemistry
ISH	in situ hybridization
kDa	kilo Daltons
LFB	Luxol Fast Blue
LV	lateral ventricle
MBP	myelin basic protein
ME	medium eminence
mfb	medial forebrain bundle
MOG	myelin-oligodendrocyte glycoprotein
MPA	medial preoptic area
MRI	magnetic resonance imaging

MS	multiple sclerosis
OL	oligodendrocyte
OPC	oligodendrocyte precursor cell
PBS	phosphate buffered saline
PCR	polymerase chain reaction
PDGFR-α	alpha-type platelet-derived growth factor receptor
PedHy	peduncular hypothalamus
Pi	pituitary
PIR	piriform area
PNS	peripheral nervous system
qPCR	quantitative polymerase chain reaction
RSP	rostral secondary prosencephalon
RT	reverse transcription
SDS-PAGE	sodium dodecyl sulphate polyacrylamide separation gel
SEM	standard error of the mean
TBS	Tris buffered saline
TBST	Tris buffered saline containing 0.1% Tween-20
Tg	transgenic
WT	wild type

CHAPTER 1: INTRODUCTION

1.1 The Nervous System

1.1.1 Overview

The nervous system is a network in all vertebrates that regulates, modulates and connects other organ systems. Moreover, the human nervous system is the most complex product resulting from biological evolution on this planet. The nervous system (NS) is the most critical of all of the organ systems and is subdivided into two major divisions: the central nervous system (CNS) and the peripheral nervous system (PNS). Whereas the CNS contains the brain and spinal cord, the PNS contains all of the other nervous tissues, including the cranial nerves, the spinal nerves, the autonomic nervous system and sensory receptors.

The CNS is made up of two types of cells: neurons and glial cells. The neuron is the basic functional unit in the nervous system. It processes and transmits information by electrical-chemical signaling. The human brain contains approximately 20 billion neocortical neurons. This large number of neurons is organized into clusters or diffused throughout the CNS, while in the PNS they are more likely to be organized together into structures called ganglia. The neurons within the same cluster or ganglion usually share the same function, the same pathway and the same signaling chemical or neurotransmitter. Despite the fact that neurons can have diverse morphologies, a typical neuron consists of a cell body, dendrites and an axon. In the classic functional model of a neuron, dendrites are branched projections that arise from the cell body and act to conduct the electrical-chemical-electrical stimulation received from other neurons to the cell body via synapses; An axon is a special cellular filament that projects from the cell body and conducts

information to its distant targets; The cell body is the information-processing centre of a neuron. The afferent information received from other neurons are integrated in the cell body of a neuron, and an efferent information is sent to its targets through the axon. In contrast, glial cells are non-neuronal support cells of the CNS and are involved in a large variety of functions including, but not limited to, the regulation of the extracellular environment and the composition of support structures. In the human brain, there are about ten times more glial cells than neurons. This ratio of neurons and glial cells is considered to be one feature that makes the human brain distinguishable from other primate brains (Azevedo et al., 2009). The glial cells consist of microglia and macroglia. Moreover, the macroglia mainly consist of oligodendrocytes and astrocytes. The activities of fully functional neurons greatly depend on the homeostatic extracellular environment that is maintained by those support cells. In general, glial cells provide structural support and nutritional supply. However, increasing evidence supports the notion that glial cells have more coordinating roles with neurons in the CNS (Wolosker et al., 2008). Compared to neurons, which are post-mitotic, glial cells have the capability of dynamic self-regeneration and strongly react after an injury to the NS. For example, a reactive astrogliosis, the condition in which astrocytes undergo hypertrophy and proliferation, can be observed in many neurodegenerative diseases, including Parkinson's, Alzheimer's, and Huntington's disease, although the roles of this astrogliosis are not yet fully understood (Allen and Barres, 2009; Aponso et al., 2008; Wolosker et al., 2008). In the early stages of MS, oligodendrocyte progenitor cells (OPCs) are generated in the edge of shadow areas of the lesion plaques where they may replenish the oligodendrocytes and the myelin (Aponso et al., 2008; Rossi and Volterra, 2009).

1.1.2 Myelin, Oligodendroglial Lineage, Myelination and Re-myelination

1.1.2.1 Myelin Sheath

The myelin sheath, which is produced by oligodendrocytes in the CNS and by Schwann cells in the PNS, is an insulating coat that wraps around the axons of neurons. In the NS, the myelin sheath acts as a shield for the axons, not only preventing the loss of electrical current but also providing a solid physical protection. This multiple-layered insulating structure is a requisite for the accuracy of nervous signal transduction. Any damage to its structure or abnormality in its normal function (referred to as demyelination and dysmyelination, respectively) will result in signal transduction problems and axonal injury, which can be found in some neurodegenerative autoimmune diseases, and hereditary and mental diseases (Zhang et al., 2008).

Lipids comprise approximately 70~85% of the dry mass of myelin (Siegel, 2006). Due to its rich lipid content, myelin looks pale in color; hence, the regions of the brain that mostly consist of myelinated axons are referred to as white matter. Although the structure and function of the myelin sheaths that are formed by oligodendrocytes in the CNS and Schwann cells in the PNS are the similar, their compositions are not identical. Generally, both have a similar lipid composition that mainly contains cholesterol, cerebroside and phospholipids. However, one distinguishing characteristic between the CNS and PNS is the difference in myelin protein composition. For instance, myelin-oligodendrocyte glycoprotein (MOG), an important antigen target in some neuronal autoimmune diseases, only exists in the CNS. This major difference in protein composition could explain why

some diseases, such as MS, only attack the myelin sheaths of the CNS, whereas demyelination in other diseases is restricted to the PNS (Brodal, 2010; Siegel, 2006).

1.1.2.2 Oligodendrogliogenesis

The process of myelination was vividly described by Mikael Simons (Simons and Trotter, 2007) as "preparing for myelination: positioning the players". Normally, oligodendrocytes arise during the development of the CNS from a pool of oligodendrocyte precursor cells (OPCs), also known as the bipotential O2A/OPC (oligodendrocyte, type 2 astrocyte precursor). These OPCs express numerous distinguishable proteins that are usually used as the cell markers, e.g., the chondroitin sulfate proteoglycan NG2, and the platelet-derived growth factor receptor subunit alpha (PDGFRα). It is known that during the cell development, NG2-positive cells and PDGFRα-positive cells share many characteristics as OPCs, and those two markers are co-localized during this period of time. However, a few researchers have questioned whether NG2 positive cells would also give rise to other cell types, aside from oligodendrocytes, in the gray matter (Ellison and de Vellis, 1994; Nishiyama et al., 1996). While the NG2-positive cells appear to have a bi-potential fate in the gray matter, there is a general consensus that the PDGFRα-positive cells are distinct from immunohistochemically identifiable astrocytes and have a high level of co-localization with NG2 in both the gray and white matter in the brain(Rivers et al., 2008). Therefore in this project, we used PDGFRα antibody to label the OPCs.

Newly generated oligodendrocytes will attach to an axon and then grow into functional mature oligodendrocytes within two to three days (Barres and Raff, 1999). It should be

noted that that oligodendrogliogenesis occurs not only during development, but also in the adult brain following injury (Chang et al., 2000; Piaton et al., 2011; Prineas et al., 1993; Rivers et al., 2008).

1.1.2.3 Myelination

Myelination is the process by which oligodendrocytes and Schwann cells produce the myelin sheaths and then wrap around the axons. In the brains of most mammals the major myelinogenesis takes place after birth till the adolescent period. Studies also revealed that a rapid accumulation of myelin related proteins occurred between postnatal 10 days and 30 days in mouse brain and the accumulation remained at a lower grade after the first postnatal month (Barbarese et al., 1978; Campagnoni et al., 1978; Morell et al., 1972). Walking is one of the native abilities of humans; however, it only becomes possible when the nerve pathways in the spinal cord become myelinated during childhood development (Davies, 2004). Moreover, most patients with MS, a common disease of demyelination, will eventually lose their ability to walk as the disease progresses.

Although myelinogenesis occurs during brain development over a relatively long period of time, the process of myelination has two major steps: the preparation of myelinating cells and the assembly of the myelin sheath.

Myelin Sheath Assembly

After newly formed mature oligodendrocytes, they begin to produce and transport myelin-related components. Due to the lipid-rich composition of myelin, the synthesis of myelin-related lipids is critical during the assembly of the myelin sheath. Cholesterol, phospholipids and glycosphingolipids make up at least 70% of the dry weight of the myelin sheath (Siegel, 2006). A early study revealed that, during brain development, the

accumulation of cerebroside, a group of nervous tissue-related lipids, paralleled the accumulation of myelin and that, although the predominant lipid for all ages of rats was cholesterol, the second most abundant lipid was cerebroside or ethanolamine phosphatide (Norton and Poduslo, 1973). Based on the correlation between lipid synthesis and myelin formation, lipid synthesis specifically cerebroside might be potentially used as a measure of the rate of myelination. This method has been tested by Jurevics et al. to evaluate the rate of re-myelination in a CPZ-induced demyelination rodent model (Jurevics et al., 2001). In addition, a close relationship had been observed between the fat composition of an animal's diet and myelin-related events (myelination, demyelination, re-myelination) (Salvati et al., 2000).

Lipids are important for myelin assembly and the majority of myelin mass, but it is the myelin proteins that make the myelin sheath functional. During the buildup of the myelin membrane, myelin proteins connect with the lipids to generate lipid-lipid or lipid-protein interactions, which help to drive lipids into more compact and dense assemblies. It is believed that myelin basic protein (MBP), a structural protein, plays an essential role for the assembly of myelin. This positively charged "sticky" protein interacts with the negatively charged cytoplasmic membrane, and this binding forces the wrapping of the myelin sheath during the myelination process. Moreover, a mutant MBP mouse strain, Shiverer (shi/shi), shows a poorly compacted myelin sheath in the CNS and an absence of the major dense lines that are normally present in the myelin sheath that give it the multiple layered appearance (Readhead and Hood, 1990) that is visible under electron microscopy (Fig. 5).

1.1.2.3 Re-myelination

The reaction of glial cells, including myelinating cells, to neurodegenerative damage is a complex processes that consists of a mixture of positive and negative responses for neuronal survival and regeneration. The responses of myelinating cells after myelin damage differ in the PNS and the CNS. In the PNS, Schwann cells proliferate after peripheral nerve injury and form a permissive microenvironment for axonal growth. The newly born Schwann cells begin to myelinate the slowly growing axons. In the injured CNS, it is now believed that the newly generated myelinating oligodendrocytes that differentiate from activated OPCs, but not those that are derived from other survived mature oligodendrocytes, restore myelin to demyelinated damaged axons (Chang et al., 2000; Rivers et al., 2008). Moreover, astrocytes become noticeably active during the demyelination and re-myelination phases. The proliferation and hypertrophy of astrocytes is often called "reactive astrogliosis," during which astrocytes increase their volume and their expression of intermediate filaments, such as glial fibrillary acidic protein (GFAP). Reactive astrogliosis has positive and negative effects on re-myelination. Reactive astrocytes release factors including growth factors and anti-inflammatory cytokines, such as interleukin-6 which activate OPCs and enhance regeneration of oligodendrocytes. However, reactive astrogliosis also leads to the release of pro-inflammatory cytokines and other inflammatory factors that interfere with axonal regeneration and contribute to local brain inflammation during both demyelination and re-myelination.

1.2Neuroendocrine System

1.2.1 Overview

The neuroendocrine system is comprised of the hypothalamus and pituitary gland and is under the influence of neurotransmitters. It is actually an integrated communicational unit combining two systems, the nervous system and the endocrine system, that interact with each other to enable the body to respond appropriately to internal and external changes. As mentioned above, the nervous system generally conducts information and command signals in a rapid fashion. Conversely, the endocrine system, which is controlled by and influences the nervous system, communicates in a slow and long-lasting fashion based on the effects of hormones. Generally, the neuroendocrine system participates in the primary regulation of bodily homeostasis and controls emotional states, body temperature, metabolism, electrolyte composition of fluids, and reproduction, among other functions (Hiller-Sturmhofel and Bartke, 1998).

1.2.2 Hypothalamus

The hypothalamus (Hypo) is the nervous system component of the neuroendocrine system and links the nervous system and the endocrine system. Anatomically, the Hypo is a CNS structure made up of distinct nuclei; there are more than ten different hypothalamic nuclei involved in many vital body functions. It makes connections with many parts of the CNS, including the brainstem, the limbic forebrain, and the cerebral cortex and thus can respond to many different signals from the CNS or the external environment. In addition, the Hypo contains connections to the endocrine system. The neural projections from the paraventricular and supraoptic nuclei that produce and secrete oxytocin and vasopressin, extend to the posterior pituitary, while other nuclei release certain hormone-releasing hormones into the hypothalamus-hypophyseal portal tract that connects the Hypo and the Pi, affecting the release of hormones from the Pi gland (Hiller-

Sturmhofel and Bartke, 1998). Moreover, the Hypo is one of the areas with an attenuated blood-brain barrier (BBB), and the primary neurotransmitters that are used as the chemical signals in the Hypo are neuropeptides (Palkovits, 1992). Unlike steroids, amino acid derivatives and other nutrients for brain metabolism, most neuropeptides cannot penetrate the BBB due to their low lipid solubility (Pardridge, 1983).

1.2.3 Pituitary gland

The Pi gland belongs to the endocrine system, and it is located directly below the Hypo. The gland consists two parts: the anterior and posterior pituitary. The anterior part of the gland produces and secretes several important hormones into the circulating blood stream where they are delivered to the target organs and cells (Houben and Denef, 1994), e.g., growth hormone (GH), prolactin, adrenocorticotropic hormone, and thyroid-stimulating hormone. In contrast, the posterior pituitary is actually a large collection of neural projections from the Hypo that stores and releases two hormones: oxytocin and vasopressin. As in the Hypo, the absence of the BBB is another important feature of the posterior pituitary. Instead, there exists a blood-cerebrospinal fluid barrier, which is more permeable than the BBB, allowing for a greater exchange of chemicals between the neuroendocrine system and the peripheral systems and is essential for the neurosecretory functions of the Pi gland.

1.3 Galanin

1.3.1 Molecular Structure

Galanin (GAL) is a biologically active neuropeptide that was initially isolated from porcine intestine in 1983 (Tatemoto et al., 1983) and is widely distributed throughout the nervous system. The sequences of the GAL peptide from several species show that GAL is a 29 amino acid-long peptide in most mammals and 30 amino acids in humans. Sequence analyses reveal that there is a complete sequence conservation of the 15 amino acids in the N-terminal in all known species. also It has been suggested that the considerable protein sequence conservation among species is consistent with conserved in basic physiological functions in the body.

GAL is produced by the proteolytic cleavage of its precursor molecule called preprogalanin. Preprogalanin contains three known peptides: a signal sequence, GAL and the galanin message-associated peptide (GMAP). Initially, GAL was believed to have no other family members besides the two proteolytic products, GAL and GMAP, until a third family member, galanin-like peptide (GALP), was discovered in 1999 (Ohtaki et al., 1999), and a fourth, alarin, in 2007 (Santic et al., 2007).

1.3.2 Expression and Regulation of GAL

Revealed by Dr. Vrontakis and Dr. Kaplan in previous studies, GAL is believed to be encoded by a single-copy gene, and the mRNA migrates as a single band of approximately 900 nucleotides in a northern blot assay (Kaplan et al., 1988; Vrontakis et al., 1987). A study of the organization of human preprogalanin gene revealed that human preprogalanin mRNA is encoded by six exons. The first encodes the 5'-untranslated region; the second exon encodes the signal peptide; the third and fourth exons encode the GAL mRNA; the remaining part of the fourth exon together with the full fifth exon and part of the sixth exon encode the mRNA of GMAP (Evans et al., 1993).

GAL is expressed predominately in the Hypo and in the gastrointestinal tract, where it was originally discovered. However, in the CNS the expression of GAL is not evenly distributed. The highest concentration of GAL is found in the Hypo with a lower level of expression in cortex and other areas in all species studied. As discussed before, neuropeptides are vital for the normal modulatory and regulatory functions of the Hypo. The neuroendocrine neurons in the Hypo can be further subdivided into the small-sized parvicellular neuroendocrine neurons and the large-sized magnocellular neurons and the interneurons that project centrally to other regions of the brain. Some early studies have studied the distribution of GAL expression in those neurons in animals (Mechenthaler, 2008; Merchenthaler et al., 1993). In the rodent, there are four groups of GAL-positive cells. A prominent cluster of positive cells is in the medial preoptic area (MPA), extending from the medial preoptic nucleus to the supraoptic nucleus. The second and third groups of cells are located in the suprachiasmatic nucleus and the periventricular preoptic nucleus. The last cluster of cells is located through lateral aspects of the MPA projecting to three destinations: the lateral preoptic nucleus, the medial forebrain bundle (mfb) and the anterior hypothalamic nucleus. There, both magno- and parvicellular subdivisions of the cells contain GAL, where they extend to other regions of the brain, e.g., some parvicellular subdivisions project to the median eminence (ME) (Merchenthaler, 1991), the brainstem and the spinal cord, while other magnocellular subdivisions project to the Pi and the brainstem (Meister et al., 1990; Villar et al., 1990). Merchethaler et al. also pointed out in their review (Merchenthaler et al., 1993) that the densest accumulation of GAL positive fibers and terminals in the Hypo is in the ME, where GAL is released into the portal circulation and then diffuses to affect the release of

hormones from the anterior pituitary. Besides the dense accumulation in the ME, a large number of fibers can also be found in the Hypo among numerous nuclei. This rich network of fibers indicates that GAL plays wide and diverse physiological roles in the neuroendocrine system.

Overall, the expression of GAL follows the manner of neuropeptide expression. According to Hökfelt et al., the pattern of neuropeptide expression can be categorized into at least three types (Hokfelt et al., 2000). First, some peptides are expressed at relatively high levels under normal conditions, indicating a consistent function. Second, the expression levels of some peptides remain very low or undetectable under the normal conditions, but they are inducible and thus will be upregulated and become functional after certain types of stimulation, e.g., nerve injury or steroid hormone stimulation. Third, some peptides are expressed at relatively high levels during the development of certain systems, often during the prenatal period, and then they are downregulated postnatally or after the maturation of the tissues in which they were initially highly expressed. Interestingly, there is a growing body of evidence showing that the expression of GAL falls into all three of these patterns.

Normally in the adult brain, the expression of GAL is high in hypothalamic neurons. GAL-rich immuno-positive fibers are widely distributed among nuclei in the Hypo. The high expression of GAL in the Hypo is a prerequisite for its consistent hypothalamic modulatory effects. For example, it is known that hypothalamic GAL participates in the regulation of the secretion of Pi hormones, the regulation of feeding and metabolism, the regulation of osmotic balance, and the regulation of the sleep-awake cycle (Mechenthaler,

2008; Merchenthaler, 1991; Vrontakis, 2002). In addition, further roles of GAL under normal physiological conditions are still being studied.

GAL is an inducible peptide, and its expression level can be dramatically upregulated under certain physiological stimulation or pathological challenges. Like the second form of neuropeptide expression as described by Hökfelt et al., the expression level of GAL in other regions of the nervous system outside of the Hypo is relatively low, or even undetectable, such as the cerebral cortex and dorsal root ganglia (DRG) neurons under normal conditions. However, after the experimental transection of the sciatic nerve, the expression of GAL in the affected DRG neurons was found to be dramatically increased (Hokfelt et al., 1987; Villar et al., 1989). Furthermore, the up-regulation of GAL was also found in neurons after experimental transient forebrain ischemia or excitotoxin-induced injury in the hippocampus (Elliott-Hunt et al., 2004; Hwang et al., 2004). In contrast, the infusion of nerve growth factor following sciatic nerve injury can suppress approximately half of the GAL expression in DRG neurons (Verge et al., 1995), while one study reported that under normal conditions, the chronic intracerebroventricular infusion of NGF strongly induced the expression of the GAL gene in adult rat basal forebrain cholinergic neurons (Planas et al., 1997). Another stimulus that has the capability to boost GAL expression in the Hypo and Pi is estrogen. Vrontakis et al. and other groups have revealed that estrogen strongly stimulates the expression of GAL in the rat Pi in a dose- and time-dependent manner. This stimulation effect was rapid but reversible (Vrontakis et al., 1989). Moreover, under normal conditions, the expression level of GAL in the anterior pituitary differs from the level in the posterior pituitary. The level of GAL mRNA in the anterior pituitary is nearly undetectable in adult male or

ovariectomized adult female mice, while the posterior pituitary, which receives nerve projections from the Hypo, contains relatively high levels of GAL in that same experimental mice. However, the administration of estrogen dramatically up-regulated GAL gene expression and peptide concentration in the rat anterior pituitary ,and to a lower extent in the Hypo (Vrontakis et al., 1989). Thus, GAL had once been believed to be an inducible hypophyseal peptide.

A gene expression map of the developing mouse brain by the Allen Institute based on the in situ hybridization (ISH) method reveals that the pattern of GAL expression during the development of the CNS is dynamic (http://developingmouse.brain-map.org/data/Gal.html?ispopup=true). Briefly, it reveals that the noticeable expression of GAL in the rostral secondary prosencephalon (RSP) and peduncular Hypo (PedHy) begins at the age of embryonic day 18.5 (E18.5), with a peak at the age of postnatal day 14 (P14). Interestingly, the expression of GAL is detectable from P4 to P14, and the level cannot be detected at P28. Another critical observation of the dynamic expression of GAL during the development of the CNS was reported by Shen et al. Their observations showed that the transient increase in GAL expression parallels the myelination of the corpus callosum (CC) during the development of the CNS from P5 to P40, in which the expression level reached the peak at P20 and thereafter returned to a relatively low level (Shen et al., 2005). The involvement of the short-term up-regulation during myelin development suggests a relationship between the effect of GAL and the synthesis of myelin or myelinating cell development.

1.3.3 Galanin Receptors

The diverse biological effects of GAL are mediated via three known receptors, galanin receptor 1-3 (GalR1-3). The features of these three receptors have been studied using molecular cloning and pharmacological techniques. All three receptors belong to the G-protein-coupled receptor superfamily, and all of them share high affinity binding for the GAL peptide. Furthermore, the affinity between galanin and a given subtype of receptors is also similar among the species tested. However, within a single species, the sequences of three receptors have relatively low homology. Furthermore, the activation of different receptors shows distinct biological roles. The full understanding of the activation pathways is still under investigation. To date, it is known that GalR1 and GalR2 signal through multiple types of G-protein subunits affecting distinct protein kinase pathways (see review (Lang et al., 2007)), while the signaling of GalR3 is poorly understood.

Due to the lack of adequate antibodies to the receptors, the localization of the receptor proteins is poorly defined. Additionally, pharmacological studies have yet to develop non-native ligands to galanin receptors (GalRs) (Lu et al., 2005). However, some characteristics have been revealed with measurements of mRNA expression both in terms of location and expression level using probing techniques, i.e., in situ hybridization (ISH) and reverse transcription polymerase chain reaction (RT-PCR). In the rodent brain, GalR1 and GalR2 are widely expressed in the brain, the spinal cord and the DRG. In contrast, the mRNA of GalR3 is predominantly presented in the peripheral tissues, while in the CNS its distribution is restricted to limited areas, mainly in the preoptic/hypothalamic area (Mennicken et al., 2002).

1.4 Multiple Sclerosis

MS is an autoimmune disorder of the CNS manifesting as acute focal inflammatory demyelination and axonal loss with limited re-myelination. MS is the most common cause of neurological disability affecting young Canadian adults. The average age of diagnosis is 37 years of age. The incidence rate of MS is 133 out of every 100,000 people in Canada between 2005 and 2006, the fifth highest rate among countries reported in an international survey (2006). Through great progress in medical care, the mean life expectancy of a patient with MS now is the same as the average population. However, up to 60% of patients are not able to walk independently 20 years after the onset of the disease. MS is a devastating and debilitating disease with which patients may suffer from almost any neurological symptom. Moreover, one subtype of MS, called the primary progressive MS, can cause serious disability or even death in a very short period of time. To date, there is no known cure for MS. The goal of treatment is to control the symptoms and postpone the disability.

1.4.1 Classification

MS has been standardized to four subtypes according to different clinical patterns of progression: relapsing remitting, secondary progressive, primary progressive, and progressive relapsing (Lublin and Reingold, 1996; Stuve and Oksenberg, 1993). However, a single progression of MS may not be restricted to one subtype of classification. Relapsing remitting MS is the most common subtype, and more than 80% of MS patients present this type of clinical pattern. It is also called benign MS, in that patients get periods lasting months to years of symptom-free remission between relapses, although the disability will eventually develop further. Up to 65% of patients with relapsing

remitting MS will eventually move to secondary progressive MS. This subtype is sometimes referred to galloping MS, in which the impairment of neurological functions and clinical symptoms begin to aggravate between each attack. Another 10~20% of patients are diagnosed with primary progressive MS, in which the neurological decline progresses from the onset of disease with short or no remission. The last subtype, the progressive relapsing, is the least common. Unlike primary progressive MS, in which there is no clear attack and remission, patients suffering with progressive relapsing will have obvious attacks but still almost no remission during the progression of the disease. In addition, other subtypes are also considered, but principally they are derived from these four.

1.4.2 Epidemiology and Etiology

MS is specifically distributed geographically worldwide. The prevalence of MS is significantly higher in the higher latitudes of the northern and southern hemispheres compared to lower latitudes close to the equator. Its prevalence is commonly higher in higher latitudes where the light/dark cycle changes due to the seasonal fluctuations in the average hours of sunlight. MS is also predominantely a disease of the western hemisphere. Above all, it is a disease that is prevalent in Europe, North America, Australia and New Zealand. Although MS is occasionally reported in China, Japan and other Asian countries, its incidence is markedly low. Often, patients with MS in those countries are misdiagnosed with other neurological diseases. The triggers for MS are still poorly understood. It is known that MS is most likely caused by a combination of genetic, environmental and infectious factors. However, the greatest known risk factor is the

female gender. The female to male ratio varies from country to country and from survey to survey. In Canada, the female to male ratio by year of birth has been increasing for at least 50 years and now exceeds 3.2:1 (Orton et al., 2006). The female gender raises the susceptibility of being diagnosed with MS, but a female with MS suffers fewer severe symptoms than males do. Moreover, many more male patients with MS develop the severe subtypes, i.e., primary progressive MS and progressive relapsing MS.

It is also noteworthy that pregnancy appears to have a strong protective effect on women with MS, and significant clinical improvement has been observed during the second and third trimesters. Oral estriol (E3) therapy administered to women with MS has also been shown to lead to a decrease in the number of lesions observed by magnetic resonance imaging (MRI) (Sicotte et al., 2002).

1.4.3 Signs and Symptoms

Patients with MS may suffer almost all neurological symptoms. In the clinic, many nervous system diseases share signs and symptoms with MS, thus the diagnosis is generally based on ruling out other conditions. Sadly, almost all MS patients will develop visual problems, mobility problems, and cognitive problems. Nevertheless, almost all of the major systems can be impaired because nearly all of the organs are connected to and contain nervous tissues. In some cases, MS can even cause fatal complications, such as choking and paralysis, by affecting vital neurological functions.

1.4.4 Pathology

BBB breakdown. The BBB is a barrier system in the CNS that normally blocks immune cells and other large or hydrophilic molecules from entering the extracellular matrix of the CNS. Sometimes, MS is also referred to as a multifocal perivascular infiltrative disease. The infiltrating material is predominantly comprised of lymphocytes and macrophages. The abnormal invasion of activated lymphocytes through the impaired BBB is the critical event to the pathogenesis. Some of the currently available treatments for MS target the adhesion molecules to decrease the inflammation-induced infiltration (Csepany, 2011).

Abnormally activated immune system. The abnormal activation of the immune system is believed to be the trigger of MS, although it is unclear what initially triggers this activation. In humans, the immune system is comprised of the innate and adaptive immune system. The innate immune system contains the phagocytic cells that defend the body against infectious organisms in a non-specific manner. The adaptive immune system works via a more complex mechanism. It mainly consists of B-cells, T-cells and molecules made by these two cell types. In terms of MS pathogenesis, both types of immune systems are involved, but it is the T-cell-mediated immune reaction that initiates the auto-immune demyelination. Normally, the adaptive immune system is essential for the homeostasis of the body's defense system. Under normal homeostasis conditions and due to a complex and delicate regulation within the immune system, the circulating lymphocytes are tolerant of self-antigens and non-tolerant or low-tolerant to foreign antigens, which means that the lymphocytes can bind to and recognize an antigen from its own body, but the immune reaction will not be activated. However in MS, for reasons that remain unclear, the tolerance to self-antigens is lost or weak. The immune system is

therefore activated by its own tissue, i.e., antigens of myelin related protein, causing the proliferating and activated lymphocytes to recognize and attack its own myelin tissues (Olek, 2005). Approximately 95% of MS patient have oligoclonal bands in the CSF but not in serum, indicating intrathecal immunoglobulin synthesis and activated immune processes in the CNS. The presence of oligoclonal bands in the CSF combined with their absence in the serum is an important indicator for the diagnosis of MS.

Demyelination. It is thought that activated lymphocytes penetrate into the brain tissue through the impaired BBB and then trigger the immune responses to myelin and other nervous tissue. Principally, the abnormally activated immune system recognizes and attacks myelin via T-cell-mediated cytotoxic and B-cell-induced humoral pathways. The immune response is complex, and it includes almost all of the immune pathways in the CNS, e.g., the complement cascade, antibody-mediated phagocytosis, $CD8^+$ T-cell-mediated direct reaction and $CD4^+$ T-cell-mediated cytokine inflammation, among others (Navikas and Link, 1996). Briefly, the inflammatory demyelination in MS results from inflammation, swelling, and lesions of the myelin in the CNS. Then the impairments lead to the abnormal transmission of electrical impulses through the axons. This signal transduction impairment leads to difficulties in the normal functions of the CNS, such as motor skills, cognition and sensation. Demyelination is the last step of the pathogenesis of MS, thus it seems that all other abnormalities eventually lead from this pathology.

Abortive re-myelination. Re-myelination is an innate ability of the adult CNS to repair itself following the pathological loss of myelin. Histological staining of tissue sections from the brains of MS patients demonstrates demyelinated plaques coexisting with re-myelinating areas or so-called shadow areas (Zhang et al., 2011). This observation

illustrates the key point that, during the process of demyelination, spontaneous re-myelination can also occur. Moreover, this recovery effect is thought to be one of four mechanisms contributing to the remission of MS symptoms, and the other three mechanisms are the resolution of the inflammation, redistribution of axolemmal sodium channels and compensatory adaptation of the CNS (Bjartmar and Trapp, 2001). However, as the disease progresses this process fails, leaving axons chronically demyelinated.

1.4.5 Treatments and Future Perspectives

According to the pathology of MS, treatment strategies can theoretically fall into two broad categories: regulating the autoimmune reaction and protecting the nerve tissues. At present, all FDA-approved treatments and most undergoing clinical trials aim to suppress or modulate the autoimmune response of MS. Despite the positive benefits of the current disease-modifying drugs for MS, they are only partially effective in preventing the onset of disability, and these immune interference treatments are not effective in the long term. Inflammation and de-myelination are hallmarks of MS, and it is the de-myelination that plays a role in causing neurological symptoms and the exacerbation of the disability. Therefore, strategies for protecting nervous tissue especially the myelin sheath are desperately needed (Buck and Hemmer, 2011). In MS, the core of neurodegeneration in the early phase is the demyelination. Thus, either preventing myelin damage or promoting the formation of new myelin will contribute to neuroprotection.

1.4.6 Animal Models of MS

Many animal models are currently available for studying MS. However, like any animal disease model, none is perfectly able to represent all features of MS in humans, although some commonly used models may mimic one or several parts of the pathogenesis of human MS. More importantly, each has a specific advantage. The most commonly used model is experimental autoimmune encephalomyelitis (EAE). It is an immune-mediated inflammatory demyelination model that is frequently used for studying the pathogenesis of the immune reaction and the inflammatory process (Lassmann, 2008). The involvement of the autoimmune reaction makes EAE an ideal model to study the classic immune regulation strategy for treating MS, but this also makes it too complex to study the demyelination and re-myelination process. Therefore, to rule out the interference of an autoimmune reaction, the CPZ-induced demyelination animal model is widely used to focus on the study of demyelination and re-myelination (Matsushima and Morell, 2001). CPZ is a copper chelator, which was initially considered for quantitative determination of copper (Nilesson, 1950). Recently, it is believed that after feeding with CPZ the copper and zinc homeostasis in a rodent brain can be severely altered (Zatta et al., 2005). Then the energy metabolism of nerve cells will be inhibited (Venturini, 1973). It is still not very clear why CPZ specifically insults OLs without obvious damage to other cell type in CNS, although an obvious hypothesis is that OLs have to maintain a vast expanse of myelin and this large metabolic demand makes OL more susceptible to be insulted if the demand cannot be met. The spontaneous re-myelination after withdrawal of the toxin makes this model useful for studing re-myelination. Most importantly, this model also

does not involve an autoimmune reaction because the administration of CPZ does not trigger an immune response.

CHAPTER 2: HYPOTHESES AND AIMS

Hypotheses

1. In GAL Tg mice, GAL will attenuate demyelination and promote re-myelination in the CPZ-induced mice model of MS.
2. Administration of estrogen to male mice will stimulate the expression of GAL and enhance the neuroprotection in the CPZ-induced model of MS.

Specific Aims

1. To determine if CPZ-induced demyelination is attenuated in GAL over-expressing transgenic mice.
2. To determine if the recovery after a prolonged CPZ-induced chronic demyelination is better in GAL over-expressing transgenic mice.
3. To determine if the estrogen treatment will further attenuate the CPZ-induced demyelination.
4. To investigate the pattern of GalR1 and GalR2 gene expression in the demyelination and re-myelination phases in the CPZ-induced model of MS.

CHAPTER 3: MATERIALS AND METHODS

3.1. Experimental Animals

All mice, including C57BL/6NCRL WT and Tg mice, were housed in the University of Manitoba animal facility in a temperature controlled environment at 20 °C on a 12 h light/dark cycle. Food and drinking water were available ad libitum. WT mice were obtained from Charles River (Montreal, QC, Canada); Tg mice were generated during our previous project using a 320-bp fragment of the rat growth hormone (GH) promoter fused to the rat full length preprogalanin cDNA clone, including its poly A tail, followed by the poly A tail of the rat GH gene (Fig. 1). Founders were on a C57BL6×SJL F2 background. Male homozygous offspring from the colony were back-crossed for at least six generations into the C57BL/6 background. Because Dr. Vrontakis et al. used the rat GH promoter, the transgene was designed for targeting to the somatotrophic cells in the Pi gland (Perumal and Vrontakis, 2003). In GAL over-expressing transgenic (Tg) mice, the circulating concentration of GAL, prolactin, GH, total cholesterol and triglyceride are significantly higher than those in WT mice (Perumal and Vrontakis, 2003; Poritsanos et al., 2009). All mice used in this study were males to avoid the effects of fluctuating steroid hormones on the expression of GAL in female mice. All procedures were in accordance with the Animal Protocol Review Board of the University of Manitoba.

3.2. CPZ-induced Demyelination

To obtain pronounced demyelination, the dose of CPZ used in this study was adjusted to 0.3% compared with the commonly used 0.2% based on a preliminary trial. No lethality was observed. To induce demyelination, both WT and Tg mice were fed a diet containing 0.3% (w/w) CPZ (Cat#: C9012-25G, Sigma-Aldrich) for 6 weeks. To induce prolonged demyelination, the CPZ exposure time was extended to 12 weeks to suppress the ability

of re-myelination. CPZ powder was well blended into milled LabDiet rodent chow (Prolab® RMH 3000 5P00, crude protein 22.0%, crude fat 5.0%, crude fiber 5.0%, ash 6.0%, added minerals 2.5%) with a food processor (Product #: 43-1976-0, KitchenAid). The blended food powder was then mixed with double distilled water. Wet diet powder was re-pelleted by extrusion through a 30 ml plastic open cylinder. The pellets were approximately 2 cm × 5 cm (diameter×length) in size. The CPZ diet was freshly prepared and served twice a week. To allow for re-myelination, the animals that received CPZ challenges were fed normal chow diet again for an additional three weeks. All of the experimental mice, both WT and Tg mice were divided into the following groups:

(1) Control group (CLT): fed with normal rodent chaw;

(2) Demyelination group, including 6-week demyelination and prolonged demyelination groups (6wCPZ and 12wCPZ);

(3) Demyelination combined with estrogen group (E3+6wCPZ); and

(4) Re-myelination groups, including recovery from 6-week demyelination, recovery with estrogen from 6-week demyelination and recovery from prolonged demyelination groups (6wCPZ+3wR, 6wCPZ+E3+3wR and 12wCPZ+3wR).

Body weight and general behaviors (e.g., grooming and activity, among others) were monitored twice a week.

3.3. Administration of Estrogen

Estrogen pellets were purchased from Innovative Research of America (Cat. No. E-141, Estriol, 21-day release, 7.5 mg/pellet). The pellet was implanted subcutaneously into the back of the neck. The procedure was performed in the operation room of the animal

center care at University of Manitoba. A dose of 0.2 ml carprofen per mouse was given for the postoperative pain control via subcortical injection 10 min before the operation. Then animals were deeply anesthetized through the inhalation of 3.5% isoflurane mixed with medical grade oxygen. After shaving the fur, sterilization was applied to the operative area. A pellet size-matched incision was made in the skin of back neck using a heat-sterilized scissors. Next, one estrogen pellet was implanted under the skin about 1.5 cm away from the cut by a pellet driver (Precision Trochar, Cat.No. MP-182, Innovative Research of America). The wound was closed with a wound clip (reorder No. 7631, Clay Adams). The clips were removed after one week.

3.4. Tissue Collection

Mice were anesthetized by isoflurane inhalation.

For Immunohistochemistry (IHC), animals were intracardially perfused with 50 ml of 0.1 M phosphate buffered saline (PBS, pH=7.4) containing 50 units/ml heparin sodium followed by 50 ml 4% paraformaldehyde prepared in 0.1 M PBS (pH=7.4). Following decapitation, the frontal, the parietal, the interparietal and the occipital bones of the skull were carefully removed to fully expose the brain by a micro bone rongeur. Then a small flat medicinal ladle was used to harvest the brains. The removed brains were post-fixated in the same fixation solution at 4 °C overnight to ensure that all brain tissues were equally fixed. The next day, the fixed brains were cryoprotected in a hypertonic buffered solution consisting of 0.1 M PBS and 30% sucrose at 4 °C until the brains sunk to the

bottom. Then the brains were snap frozen on dry ice and stored at -80 °C until the frozen section applied.

For Luxol fast blue (LFB) staining, the tissue collection procedure was the same as for IHC prior to the cryoprotective treatment with 30% sucrose solution. Instead, after post fixation at 4 °C overnight, the brains were immersed in 0.1 M PBS containing 8% sucrose at 4 °C to wash the brain tissue for another 24 h.

For electron microscopy (EM), after anesthesia, animals were intracardially perfused by a perfusion pump (Low-Flow Peristaltic Pump, Cat#. 13-876-1, Fisher Scientific) for a stable flow perfusion. First, the blood was removed by perfusion with 0.1 M PBS containing 50 units/ml heparin sodium at a speed of approximate 8 ml/min for 5 min. Then animals were fixed by perfusion with buffered (pH=7.4) EM fixation solution containing 2% paraformaldehyde, 2% glutaraldehyde and 0.1 M PBS was administrated at a speed of 3~4 ml/min for 20 min. After fixation, the brains were collected using the same method as the described above for IHC. In the brain holder, several 1~2 mm thick coronal sections were made. The sections were then further fixed in 0.1 M Sørensen's buffer (a double strength Sørensen's buffer, pH=7.4, is prepared by mixing 5.24 g $NaH_2PO_4 \cdot H_2O$ and 23.0 g $Na_2H\,PO_4$ with 1000 ml ddH_2O) containing 3% glutaraldehyde at room temperature for 3 h. The fixed samples were washed by immersion in 0.1 M Sørensen's buffer containing 5% sucrose at 4 °C overnight. The next day, the samples were further washed in 0.1 M Sørensen's buffer containing 5% sucrose two times for 40 min each at room temperature on an orbital shaker. After the final washing, samples were

stored in 0.1 M Sørensen's buffer containing 5% sucrose at 4 °C until post-fixation with osmium tetroxide was applied.

For gene expression analysis, the brains were removed in a similar fashion as described for IHC. However, following the administration of anesthesia, the animals were quickly decapitated without perfusion, and then the brains were collected. Compared to the collection method for IHC, harvesting the brain as soon as possible is critical for gene expression analysis because RNA is unstable and quickly degrades. To limit the degradation, all surgical instruments used for dissecting tissues for gene expression analysis were made RNase-free by cleaning with RNaseZap® (Cat#: 9780, Ambion). After the fresh brains were removed, they were placed on ice in a stainless steel mouse brain holder (Adult Mouse Brain Slicer Matrix, Cat#: BSMAS005-1, ZIVIC Instruments). Then the Pi gland was carefully collected using fine forceps. For each brain, several 2.5 mm thick coronal sections were obtained from consistent locations as follows.

For CC, the first coronal cut was 5 mm away from the edge of the olfactory bulb, and the second cut was 2.5 mm (5 slice section intervals of the brain holder) away from the first cut. Then the brain structures representing the CC and part of the cortex were dissected from the brain section on ice under a stereomicroscope (Fig. 2).

For the Hypo, the first coronal edge of the brain tissue section was the second cut as described above for the CC, and the second cut was made another 2.5 mm away from the first edge. The area containing the Hypo was collected under a stereomicroscope.

Isolated tissues, including Pi, CC and Hypo, were separately transferred to 1.5 ml RNase-free tubes (Cat#. 0030 120.086, Eppendorf) containing 1 ml of RNAlater® solution to

prevent degradation of the RNA (Cat#. AM7020, Ambion). Then samples were incubated at 4 °C overnight to allow for the complete penetration of RNAlater® solution. Treated samples were then stored at -80 °C until the RNA extraction procedure was performed.

For the western-blot analysis, tissue collection was similar to that performed for gene expression. Dissected cortex samples were stored directly in clean autoclaved tubes at -80 °C until the protein extraction procedure was performed.

3.5. Tissue Preparation

For IHC, serial coronal sections (25 μm thick) were cut from the frozen brains using a Leica SM2400 sliding microtome equipped with a freezing plate set to -30 °C. The free-floating sections were then kept in 24-well plates containing 0.1 M PBS at 4 °C. The sections were transferred into a cryoprotection solution containing 30% glucose and 30% ethylene glycol in 0.1 M PBS for long-term storage. Sections at the 185 to 195 levels according to the High Resolution Mouse Brain Atlas by Sidman et al. (http://www.hms.harvard.edu/research/brain/atlas.html) were used for IHC staining.

For LFB, the brains were embedded in paraffin. The brains were transferred into tissue processing cassettes, and then the cassettes were put into a beaker containing 70% ethanol. The dehydration process was performed with an automatic tissue processor (Shandon Citadel Tissue Processor, Department of Human Anatomy and Cell Science, University of Manitoba). The dehydration process was completed the next day with a finishing step of the infiltration of hot wax at 60 °C to embed the brain tissues in paraffin.

The paraffin blocks were stored at -20 °C until cut. For LFB, 6 μm thick sections from the similar levels of the brain used for IHC were cut using a paraffin microtome. The paraffin sections were stored in the section case at room temperature until staining was performed.

For EM, the brain sections were transferred onto a clean glass slide. Several 1×1×1 mm tissue blocks were made using an ethanol-treated oil-free single edge blade. The tissue blocks were then post fixed for 1~2 h in 1% osmium tetroxide prepared in 0.1 M Sørensen's buffer at room temperature followed by washes in 0.1 M Sørensen's buffer three times for ten minutes each. After the tissues had been fixed and washed, the complete dehydration process was performed. Tissues were treated in a graded series of alcohol: 30% 10 min, 50% 10 min, 70% 10 min, 90% 2×10 min, and 100% 3×10 min. A treatment of methanol for 20 min was applied to further remove the water from the tissues, and then the tissue blocks were incubated twice in propylene oxide for ten minutes each to replace the residual alcohol, followed by two steps of the infiltration process for 1 h each at room temperature as follows: an incubation in a mixture containing one part propylene oxide and two parts embedding medium and an incubation in a mixture containing two parts propylene oxide and one part embedding medium (Table 1). Finally, the tissue blocks were transferred into the embedding capsules (Cat#. 70000-B, Electron Microscopy Sciences) containing 700 μl pure embedding medium at room temperature for 24 h followed by the polymerization process in an oven at 60 °C for 48 h.

Table 1 Embedding medium for electron microscopy

Reagent	Volume (for approx. 5 blocks)
Poly/Bed® 812	2.5 ml
Araldite 502	2.5 ml
DDSA	6 ml
DMP-30	225 µl

All materials were provided in the Araldite 502/PolyBed 812 Kit purchased from Polysciences, Inc. The embedding medium recipe was provided with the kit. The compositions were fully mixed by a magnet stirrer for 1 h, then the mixture was incubated for another 1 h to remove bubbles.

For western-blotting, protein extraction was performed. The frozen tissues were mixed with 200 µl of protein lysis buffer (1% w/v Triton X-100, 50 mM Tris·Cl pH=7.4, 300 mM NaCl, 5 mM EDTA, 0.02% w/v NaN_3) plus 2 µl 100× protease inhibitor cocktail (CKT, Cat #. P8340-1ML, Sigma-Aldrich). Then the samples were put on ice for complete thawing. After thawing, the samples were ground by the same homogenizer used for RNA extraction. The probe was washed in clean lysis buffer three times between samples. The homogenates were then centrifuged at 18,000 rpm at 4 °C for 30 min. The supernatants were transferred into fresh clean tubes, and the protein extracts were stored at -80 °C until western blotting was performed.

3.6. RNA Preparation

Frozen RNA samples were put on ice for thawing, after which the RNAlater solution was replaced with 0.6 ml (0.4 ml for Pi samples) of ice-cold TRIzol (TRIzol Reagent, Cat#: 15596026, Invitrogen). Tissues were homogenized at full grinding speed by physical grinding (Homogenizer Power Gen 125 with Generator Flat 5x95, Fisher Scientific). The homogenizer probe was washed in 70% ethanol while running at full speed in 70% ethanol followed by three washes in DEPC-treated water between samples. The homogenized tissues were incubated at room temperature for 5 min followed by the addition of 120 µl (80 µl for Pi) chloroform. Then samples were mixed vigorously on a

vortex shaker for 25 s and incubated at room temperature for 3 min. The samples were then centrifuged at 12,000 rpm for 15 min in a pre-chilled centrifuge. As a result of centrifugation, the mixture separated into three parts: a lower red phenol-chloroform phase, a pale colored interphase, and a colorless upper aqueous phase. As RNA remains exclusively in the aqueous phase, approximately 90% of the upper clear phase was transferred into a fresh RNase-free tube. To avoid any inclusion of the interphase, roughly 10% of the aqueous phase was left uncollected. RNA was precipitated from the aqueous phase by the addition of 300 µl molecular grade isopropyl alcohol (200 µl for Pi samples). After the addition of isopropyl alcohol, the mixtures were gently mixed by vortexing and incubated on ice for 10 min. RNA precipitates formed tiny gel-like pellets at the bottom of the tube after centrifugation at 12,000 rpm for 10 min. The supernatant was carefully discarded, and the pellet was washed with 1 ml of pre-chilled RNase-free 75% ethanol by vortexing. The fragments of the RNA pellet were re-collected by centrifugation at 12,000 rpm for 5 min in the same pre-chilled centrifuge. The washed RNA pellet was then air-dried for 5 min and dissolved in 87.5 µl RNase-free water. In order to ensure reliable gene expression analysis, the total RNA samples were purified using the a total RNA purification kit (RNeasy Mini Kit, Cat. No. 74104, QIAGEN) according to manufacturer's protocol. Briefly, the genomic DNA was decontaminated by incubation with the DNase that was supplied in the purification kit at room temperature for 10 min, then raw RNA sample was transferred into RNeasy mini spin column that is supplied in the kit where the total RNA binds to the silica-based membrane and contaminants that could inhibit downstream applications are efficiently washed away.

Purified concentrated RNA samples were dissolved in RNase-free water and were stored at -80 °C until first-strand synthesis was performed.

3.7. Immunohistochemistry

Staining was performed with the avidin-biotin-peroxidase complex technique. Procedures were done on a slow shaker at room temperature unless otherwise indicated. Briefly, free-floating sections were washed in 50 mM tris buffered saline (TBS, pH=7.4) three times for 5 min each followed by a pre-treatment with 3% hydrogen peroxide for 30 min. Then sections were washed in TBS and incubated in a blocking solution consisting of 5% normal goat serum and 0.3% Triton-X100 in TBS for 1 h. Subsequently, the sections were incubated in the same blocking solution overnight at 4 °C with primary antibodies (Table 2). After washing in TBS containing 0.1% Tween-20 (TBST), sections were incubated with biotinylated secondary antibodies (all secondary antibodies were purchased from Vector Laboratories, Ontario, CA) for 1 h, followed by three washes in TBST. Then sections were further treated with an avidin-coupled biotinylated horseradish peroxidase (HRP) complex (ABC Peroxidase Staining Kit, Cat#: 32020, PIERCE) for 1 h. Finally, immuno-precipitated sections were visualized using a DAB kit (DAB Peroxidase Substrate Kit, 3,3'-diaminobenzidine, Cat#: sk-4100, Vector Lab). After the sections were transferred onto clean pre-coated slides (Fisherbrand® Superfrost®/Plus Microscope Slides Cat# 12-550-15), sections were allowed to air-dry on a 37 °C slide warmer overnight. The next day, the sections were post-treated in a series of alcohols of increasing concentration from 70% to 100%, followed by two treatments in xylene. Finally, slides were mounted with 22x40 mm cover slips by Permount. Control slides were treated at the same time using the same reagents without primary antibodies. No

positive staining was found in the control slides, which were treated with the same staining condition without the primary antibodies (graphs not shown).

Table 2 Primary antibodies used for immunohistochemical staining

	Target	Dilution ratio	Catalogue No.	Supplier
Anti-MBP	Myelin	1:1000	Sc-13914	Santa Cruz
Anti-GST-π	Mature OL	1:1000	610719	BD Biosciences
Anti-Galanin	Galanin peptide	1:500	BML-GA1161-0100	Enzo
Anti-GFAP	Astrocyte	1:1000	MAB360	Millipore
Anti-CD140a	PDGFR-α/OPC	1:500	558774	BD Biosciences

Abbreviations: MBP, myelin basic protein; GST-π, Glutathione S-Transferase π form; GFAP, glial fibrillary acidic protein; PDGFR-α, alpha-type platelet-derived growth factor receptor; OPC, oligodendrocyte precursor cell; OL, oligodendrocyte.

3.8. Luxol Fast Blue

The paraffin sections were de-paraffinized and rehydrated by the following incubation steps: xylene 2x5 min, pure ethanol 2x5 min and 95% ethanol 2x5 min each. Then rehydrated sections were incubated in 0.1% Luxol fast blue solution (LFB solution was prepared by mixing 0.1 g Luxol fast blue, 100 ml 95% ethanol and 0.5 ml glacial acetic acid) in an oven at 60 °C overnight. The stained sections were rinsed in 95% ethanol for 5 min followed by washing in distilled water for 5 min. The next step was to produce a sharp contrast between the blue of the white matter and the colorless gray matter by the differential process that included a differentiation in 0.05% lithium carbonate for 30 s, followed by another differentiation in 70% ethanol for 30 s and a rinse in distilled water. The differential process was repeated several times until the gray matter was clear and the white matter was clearly defined under a microscope. After approximately five repeats of the differential process, the sections were counterstained with 0.1% cresyl violet solution

for 40 s followed by a rinse in running distilled water for 3 min. Finally, the sections were re-dehydrated in a series of increasing grades of ethanol followed by two treatments of xylene. The slides were covered by Permount.

3.9. EM

The polymerized EM blocks were collected from the embedding capsules by a capsule press (Cat#. 69920-00, Electron Microscopy Sciences). The EM blocks were trimmed so that sections would only be cut from a small portion of the block face. After the trimming procedure, the cutting face of the block had a length of less than 2 mm to each edge.

Thick, 1 μm sections were cut manually using a diamond knife provided by Dr. J.A. Thliveris (Department of Human Anatomy and Cell Science, University of Manitoba). Sections were collected and stained with 1% toluidine blue. Under a light microscope, the desired area was identified. Thereafter, the cutting face of the EM blocks was trimmed even smaller. Then ultrathin sections were cut using a microtome. The ultrathin sections were cut floating on the water surface of the knife reservoir. The thickness was determined by the interference color of the sections; sections with silver color indicating a thickness of 50~70 nm were selected and collected onto copper grids. The grids were air-dried on filter paper and were stored in the grid case until the staining was performed.

Several drops of 5% uranyl acetate were pipetted on a wax-coated Petri dish, and the grids containing ultrathin sections were put onto the solution drops upside down for 30 min followed by three washes in water. After absorbing the residual water from the grids with filter paper, the grids were incubated with 0.2% lead citrate for 10 min followed by

three washes in water. Finally, the ultrathin sections were air-dried for 30 min and stored in the grid case until photography was performed using a Philips 201 electron microscope.

3.10. Western blotting

Protein Quantification

The frozen protein extracts were placed on ice for thawing. The protein concentration was measured using a BCA Protein Assay Kit (Product #. 23225, Pierce, Thermo Scientific). 10 µg of total proteins in a 3 µl volume were used for western blotting, thus all samples were diluted to 3.5 µg/µl with lysis buffer.

Protein Denaturing

A volume of 25 µl of diluted protein samples was mixed with 5 µl of 6× protein loading buffer (12% SDS, 30% 2-mercaptoethanol, 60% glycerol, 0.012% bromophenol blue, 375 mM Tris·Cl). The mixtures were then incubated in a boiling water bath for 3 min followed by snap-cooling on ice prior to loading on the gel.

Western blotting

A final volume of 3 µl denatured protein samples and a protein marker (EZ-Run Prestained REC Protein Ladder, Cat #. BP3603-500, Fisher BioReagents) were resolved by 15% sodium dodecyl sulfate polyacrylamide gel electrophoresis (SDS-PAGE) using a Mini Protean 3 cell system at room temperature (Cat #. 165-3301, BIO-RAD). Samples were separated in the gel under a stable running voltage set at 58 volts for 3 h, and then the voltage was increased to 80 volts for another 40 min. The separated proteins on the gel were then transferred to a PVDF membrane under a stable current at 157 mA for 2.5 h using the Mini Trans-Blot Cell system (Cat #. 170-3930, BIO-RAD) on ice. Membranes

were blocked with 5% milk in TBST buffer for 1 h and then incubated with an antibody against MBP diluted 1:1500 overnight at 4 °C. The next day, membranes were washed three times in TBST buffer and then incubated with a secondary antibody for 1 h at room temperature on a rocking shaker. The secondary antibody was further labeled with Western Lightning® Plus-ECL (Cat#. NEL104001EA, PerkinElmer). The labeled protein-antibody complexes were visualized using manual film development with autoradiography films in developing agent and fixation agent (Kodak® processing chemicals for autoradiography films, Cat#. P7042-1GA, Sigma-Aldrich). After the membrane was washed with TBST three times for 10 min each, the protein detection method was repeated with the antibody against mouse β-actin for a loading control.

3.11. Screening Genomic DNA by Polymerase Chain Reaction (Genotyping screen)

Genomic DNA was extracted from mice tails by GenCatch blood/tissue Genomic miniprep Kit (Cat#. 1460050, Epoch Biolabs) according to the manufacturer's protocol. The precipitated DNA pellets were dissolved in 50 µl. Because the genotyping screen was a qualitative not quantitative analysis, the measurement for the concentration of DNA was not routinely applied until a negative result appeared. Then a 523 bp length fragment of the transgene (Fig. 1) was amplified by regular PCR. The PCR reaction consisted of 1 µl of raw DNA sample and 49 µl of a genotyping PCR master mix (Table 3, Table 4). The PCR products were separated by electrophoresis on a 0.9% agarose gel containing 0.5 µg/ml ethidium bromide. The bands were visualized and documented with

ultraviolet light by a FluorChem-8900 chemiluminescence and gel imager from Alpha Innotech.

Table 3 Genotyping PCR master mix

Reagent	One reaction volume
Pure water	37.8 µl
10x PCR buffer	5.0 µl
25 mM $MgCl_2$	3.0 µl
10 mM dNTP Mix	1.0 µl
20 µM Gal forward primer	1.0 µl
20 µM Gal reverse primer	1.0 µl
Taq DNA polymerase	0.2 µl

10 mM dNTP Mix (Cat#. 18427-013, Invitrogen); 10x PCR buffer (P/N y02028, Invitrogen); Taq DNA Polymerase recombinant (5 u/µl, Cat#. 10342-020, Invitrogen)

Table 4 Sequence of galanin transgene primers

	Sequence
Forward primer	5'-GTACCCTGCCAGAGTATCCTA-3'
Reverse primer	5'-GCATCCCGAGCCCCAGAGTG-3'

3.12. Real-Time Reverse Transcription Polymerase Chain Reaction (real-time RT-PCR)

The qPCR was performed using a two-step reaction.

Step one: First-strand synthesis, reverse transcription (RT)

The frozen, concentrated RNA samples were thawed on ice. Then a measurement for the concentration of RNA was performed to ensure that 1 µg of total RNA was used to generate the single-stranded cDNA. (NanoDrop, Cat#: ND-1000, Thermo, Fisher Scientific). The concentrated total RNA samples were then diluted to 0.1 µg/µl in a 10 µl volume. Before mixing the diluted RNA samples with RT master-mix (Table 5), RNA samples were denatured by incubating at 70 °C for 10 min followed by mixing well with the RT master-mix. For RT, the reaction was incubated in a programmed thermal cycler

under the following conditions: 25 °C 10 min, 42 °C 50 min, 72 °C 15 min, and 0 °C until use.

Table 5 RT master-mix

Reagent	One reaction volume
Pure water	1.2 µl
5x First Strand buffer	4.0 µl
25 mM dNTP mix	0.8 µl
0.1 M DTT	2.0 µl
0.5 mM Random Hexamers	1.0 µl
40 unit/µl RNase Out	0.5 µl
200 unit/µl SSII	0.5 µl

SSII (SuperScript II Reverse Transcriptase, P/N 100004925, Invitrogen, SSII package contains 5x First Strand buffer and 0.1 M DDT); RNase Out (Ribonuclease Inhibitor, Cat#: 10777-019, Invitrogen); Random hexamer primer (Cat#: 11034731001, Roche)

Step two: Real-time PCR

Generated cDNA templates were diluted with 50 µl RNase-free water. For quantitative amplification, primer pairs with high amplification efficiency were designed and generated by SABiosciences™, QIAGEN. The housekeeping gene GAPDH (glyceraldehyde-3-phosphate dehydrogenase) was used as an internal control (Table 6). Each PCR reaction system for each gene amplification consisted of 12.5 µl RT^2 SYBR Green/ROX qPCR MasterMix (Cat#: PA-012-24, SABiosciences, QIAGEN), 6.5 µl RNase-free water and 1 µl primer mix. The PCR reactions for each gene of interest were performed in triplicate using the StepOne™ Real-Time PCR System (Applied BiosystemsTM). The PCR reaction cycling program was as follows: 95 °C for 10 min; 40 cycles of 95 °C for 15 s and 60 °C for 1 min. Melt curve program: 95 °C for 15 s; 60 °C for 1 min; 65 °C to 95 °C at 2 °C /min; and 95 °C for 15 s.

3.13. Data collecting and processing

The body weight of all experimental animals was monitored twice a week. For calculation, the first one of the two measurements was used. The body weight growth of each individual mouse was calculated in terms of percent body weight growth compared to the initial body weight.

IHC stained slides were digitally captured using a ZEISS AxioImager A1 light microscope equipped with the AxioCam ICC3 digital camera and OLYMPUS BH-2 light microscope equipped with the OLYMPUS Q-color5 digital camera. The software used with those two microscopes were AxioVision Rel. 4.8 version (Carl Zeiss) and ImagePro Plus (MediaCybernetics, 5.0 version), respectively. MBP-immunostaining revealed many fine fibers that pass through the cortex and were heavily condensed in CC. These positively stained fibers were very fine and condensed to each other, thus we measured the optical densities of MBP-immunostaining according to the NIH ImageJ protocols for quantitative comparison ((NIH)). Because the DAB color intensity varies slightly between samples due to the natural variation of DAB staining in spite of the same staining condition, the optical density measurements were color intensity-standardized using the optical density of aco, as demonstrated in Figure 3, where the MBP staining remain intact regardless of CPZ challenge. All of the data collection methods were also applied to analyze the GFAP and PDGFR-α staining because the proliferation of the positive cells in the experimental groups increased so dramatically that we could not accurately count them, while the analysis of GST-π staining was based on the actual counting of the whole field of view.

The films obtained from western blot analyses were scanned using a HP Deskjet F4280 all-in-one printer.

The real-time RT-PCR results were analyzed by the StepOne™ software version 2.1 using the comparative threshold cycle (C_T) quantitation method. This method is used to determine the relative gene expression quantity in samples. With the method, the software evaluated amplification of the target and endogenous control genes in terms of C_T value in all samples including the experimental manipulated samples and the WT control samples. The amplification measurements were normalized using the endogenous control gene, i.e. GAPDH. The software then calculated the relative quantity of target gene, i.e. GAL or its receptors, in each sample by comparing normalized target gene quantity in each sample to normalized target gene quantity in the WT mice control sample. The results were expressed as the fold-change of target genes in the samples relative to the WT mice control samples.

3.14. Statistical analysis

The statistical calculations and graphing were performed using GraphPad Prism® version 5. Body weight data were analyzed by two-factor mixed-measures analysis of variance (two-factor mix-measures ANOVA) considering the genotype as the factor for independent groups, and the time elapsed was the other factor for repeated measures. All IHC data were analyzed with two-way independent ANOVA considering the genotype to be the independent variable and different groupings for different levels of experimental manipulation as another independent factor. All two-way ANOVAs were accompanied by Bonferroni's multiple comparison tests. When considering the variances by either factor, e.g., body weight changes within WT groups, one-factor ANOVAs plus Tukey's

multiple comparison tests were applied. A p-value of less than 0.05 was considered significant. The data were expressed as the mean ± standard error of the mean (s.e.m.).

CHAPTER 4: RESULTS

4.1. In untreated Wild-type mice, axons in the brain were wrapped by multiple layered electron-dense membranes

In the cerebral cortex, myelinated axons were located in bundles, and each bundle contained different sizes of myelinated axons (Fig. 5 A), while in the CC (Fig. 5 B) myelinated axons were close to each other, and the diameters of the axons varied from 200 nm to 9 μm as measured by ImageJ software. The high magnification image enlarged 64,000 times revealed that the electron-dense membranes wrapping around the axons were multiple layered. Furthermore, the thicknesses of the myelin sheath were similar to each other as revealed in Fig. 5 C. The myelin sheath wrapping the larger axon contained many more layers of myelin lamellae, and that myelin sheath was much more condensed compared to those wrapping the smaller axons.

4.2. Effects on body weight of the over expression of GAL

Initially, at the age of 8~9 weeks old, Tg mice were heavier than WT mice, with average body weights of 29.9±4.3 g and 24.9±2.4 g, respectively (mean± standard deviation) (Fig. 6 A). By six weeks later, Tg mice and WT mice in control groups gained 27.6±18.3% and 21.3±13.5%, respectively, of their body weight compared to their initial weight (Fig. 6 B).

In comparison, after treatment with CPZ diets, both Tg and WT mice significantly lost body weight in the first week. Tg mice lost roughly 5% after one week, while WT mice lost 10% after two weeks (Fig. 7 B). However, Tg mice started to gain weight after one week, while WT mice continued to lose weight until the third week. Moreover, after withdrawal of the CPZ challenge, both genotypes of mice gained weight immediately but at different rates (Fig. 7). The body weights of Tg mice were significantly heavier than that of WT mice throughout the whole CPZ challenge (Fig. 7A). There was a statistically significant difference showing that the body weight of Tg mice increased more quickly than did WT. The two-way mixed-measures ANOVA revealed a significant interaction ($F(6,138)=9.83$, $p<0.0001$) between the normal body weight growth rate and the genotypes, meaning that the rate of body weight growth depended on the genotype. Another two-way mixed-measure ANOVA revealed that, under the CPZ challenge, there was a significant influence of genotype on changes in body weight.

4.3. CPZ-induced demyelination was attenuated in GAL Tg mice

In the sub-project of a six-week CPZ semi-acute challenge, the myelin breakdown and the related pathogenetic changes were alleviated in Tg mice (Fig. 8).

4.3.1 CPZ-induced demyelination in MBP staining was attenuated in GAL transgenic mice

As described in previous studies (Matsushima and Morell, 2001; Torkildsen et al., 2008), our findings also revealed that the CPZ challenge caused significant loss of myelin in wild type (WT) mice (C57BL/6), particularly in the CC and the junctional area between the CC and the cerebral cortex (Fig. 8 B, b). However, the myelin breakdown was

significantly reduced in Tg mice (Fig. 8 E, d). Obviously, in Tg mice, the degradation in the external capsule of the CC, as demonstrated by the arrow in the whole brain pictures (Fig. 8 b, d), was reduceed compared to WT mice, although there were some areas in the cerebral cortex where myelin staining was reduced, e.g., cortical layer two and layer five. In WT mice, after six weeks of CPZ-induced challenge, only a few myelin fibers remained in the cortex that were restricted to layer four. However, both WT and Tg mice in the recovery groups showed a dense staining of MBP (Fig. 8 C,F). A two-way ANOVA revealed that the genotypes significantly affected MPB staining among control, demyelination and re-myelination groups ($F(2,16)=9.56$, $p=0.0019$). Post-hoc comparison tests found that Tg mice had a significantly greater level of MBP staining, based on the optical density values (Fig. 9), after six weeks of the CPZ challenge. One-factor ANOVA tests on the WT mouse data revealed that the CPZ-induced challenge significantly affected the myelin staining results ($F(2,6)=28.86$,$p<0.001$). Nevertheless, we also applied Luxol Fast Blue (LFB) staining to normal and CPZ-challenged animals to verify the IHC results. And the results further provided that the integrity of myelin fibers were similar to the IHC staining (Fig. 14). The western blot analysis of MBP protein of WT mice further confirmed that after CPZ challenge for either six weeks or twelve weeks MBP protein levels were reduced then after three weeks recovery MBP protein levels recruited. Those protein level changes paralleled with the changes of MBP staining (Fig. 10).

4.3.2. Over-expressed GAL alleviated the demyelination-related pathogenesis

(1) The loss of mature oligodendrocytes was reduced in GAL over-expressing Tg mice

We first examined those mature oligodendrocytes that survived after the CPZ-induced challenge. IHC staining demonstrated that, in normal control animals, there were widely distributed GST-π positive cells in the cortex (normal whole brain photographs not shown) and linearly distributed ones in the CC (Fig. 13 A, D). As expected, after six weeks of CPZ-induced challenge in WT mice, only a few weakly positive cells remained in the CC, and a small number of positive cells remained in the cortical areas restricted to cortex layer four (Fig. 13 G), but there were still many positive cells in the Tg mice (Fig. 13 E, H). Furthermore, many positive cells could be seen in WT mice from the recovery group, while there were no obvious changes in Tg mice between the demyelination and recovery groups (Fig. 13 E, F). A two-way ANOVA on the cell counting (Fig. 13 I) revealed that the genotypes significantly influenced the number of GST-π positive cells regardless of control, demyelination and recovery conditions ($F(2,12)=4.40$, $p=0.0370$). Post-hoc comparison tests found a significant difference between WT and Tg mice from the 6wCPZ group ($p<0.01$). A one-way ANOVA test on the WT groups showed that the mean numbers of positive cells were significantly different across groups, and Tukey's test revealed significant differences between groups listed as follows: WT CLT vs. WT 6wCPZ and WT 6wCPZ vs. WT 6wCPZ+3wR. However, a one-way ANOVA test on Tg groups revealed no significant difference among groups, although the results showed a trend that indicated impairment after the CPZ-induced challenge.

(2) The proliferation and accumulation of OPCs were low in the Tg mice after CPZ-induced challenge

The distribution of OPCs was revealed by IHC for PDGFR-α, one of the two commonly used cell markers for OPCs. Under normal conditions, in the control groups there were few PDGFR-α-positive cells in the brains of WT and Tg mice (Fig. 15 A, D). After the CPZ challenge, PDGFR-α-positive cells began to increase in the CC of WT mice (Fig. 15 B). Furthermore, this positive staining was reinforced significantly in the brains of WT mice from the recovery group (Fig. 15 C), in which the challenge of CPZ was alleviated compared to either the control ($p<0.01$) or demyelination group ($p<0.05$) (Fig.15 G). In contrast with WT mice, the numbers of PDGFR-α-positive cells in Tg mice was similar among the different groups (Fig. D-F).

(3) In GAL over-expressing mice the invasion of CPZ-induced reactive astrogliosis was restricted.

Without any experimental challenge, most of the GFAP positive cells were limited to the CC area in both WT (Fig. 16 A, a) and Tg mice brains (Fig. 16 D, d). As expected, after the CPZ-induced challenge, increased numbers of GFAP-positive astrocytes could be detected in all regions of the brain in both WT (Fig. 16 B, b) and Tg mice (Fig. 16 E, e). More precisely, the distribution of the reactive astrocytes in WT mice was diffused through all layers of the cerebral cortex, but in Tg mice, the invasion of reactive astrocytes was limited within layer four of the cerebral cortex, i.e., no labeling was seen in cerebral cortex layers five and six. In the recovery groups, the reactive astrogliosis (in terms of the density of staining) in WT mice was reduced, although the distribution was still dispersed in the cortex, but the diffusion in Tg mice were still restricted in the limited regions.

4.4. Over-expression of GAL promoted myelin regeneration

Because the semi-acute demyelination induced by six weeks of CPZ challenge could not suppress the re-myelination ability after withdrawal of CPZ in both genotypes of mice, as revealed by IHC staining, it was difficult to conclude whether the over-expression of GAL had a promoting effect on re-myelination. Thus, we studied the chronic demyelination induced by a prolonged twelve week CPZ challenge to suppress the native re-myelination ability to both genotypes of animals. As expected, after twelve weeks of exposure to CPZ, Tg mice showed severe demyelination (Fig. 11 e). However after three weeks of recovery, Tg mice showed significant re-myelination (Fig. 11 f), while the WT mice showed only several re-myelination spots in the brain (Fig. 11 c).

4.5. The administration of estrogen enhanced the protective effect in GAL Tg mice

Because it had been shown that estrogen has significant neuroprotective effects (Tiwari-Woodruff et al., 2007; Tiwari-Woodruff and Voskuhl, 2009), we also found that estrogen treatment greatly alleviated myelin breakdown in WT mice (Fig. 12 C). The effect of the protection of estrogen in WT mice was similar to the effect of the over-expression of GAL in Tg mice in terms of MBP IHC staining (Fig. 12 C vs. E). However, the combination of administration of estrogen and over-expression of GAL further enhanced reducing of myelin breakdown in the Tg mice (Fig. 12 F).

4.6. Changes in gene expression

(1) The expression of GAL was regulated in different conditions in different tissues

Initially, the expression of GAL in Tg mice was suppressed half-fold compared with the levels in WT mice under normal control conditions (CLT) (Fig. 17 A and B). However, in the Tg mice, GAL was significantly over-expressed by about 400-fold in the Pi compared with in the CC in WT mice (Fig. 17 B). After the CPZ-induced challenge, the expression in the CC was up regulated, and the expression of GAL in Tg mice was significantly higher ($p<0.05$) after the recovery (Tg 6wCPZ+3wR) than under normal conditions (Tg CLT). The expression changes in WT mice in the CC between groups were not significant different due to the size of the sample. Furthermore, the expression of GAL in the CC was not affected by the administration of estrogen during demyelination (Fig. 17 A).

Compared to the expression changes in the CC between the two genotypes, the expression of GAL in the Hypo and Pi were highly induced (Fig. 18). The expression assay of WT mice revealed that the CPZ-induced challenge stimulated the expression of GAL 51-fold in the Hypo and 19-fold in the Pi compared to the expression levels in CC, while the administration of estrogen under the same CPZ-induced challenge increased the expression of GAL in WT mice 78-fold in the Hypo and 4,266-fold in the Pi compared to the expression levels in CC.

(2) The GalR1 and GalR2 differentially react during demyelination and re-myelination

The expression levels of candidate genes were normalized to the levels detected in WT mice from the control group. The expression levels of GalR1 were 2.7- and 6.4-fold higher in WT and Tg mice, respectively, in the demyelination groups; furthermore, their

expressions were increased 2.9- and 5.8-fold in recovery groups (Fig. 19 A). In contrast with GalR1 expression, the expression of GalR2 was up-regulated 1.4- and 2.1-fold in WT and Tg mice, respectively, in the demyelination groups, and the expression of GalR2 increased 2.2- and 3.3-fold in WT and Tg mice, respectively, in the recovery groups (Fig. 19 B).

CHAPTER 5: FIGURES

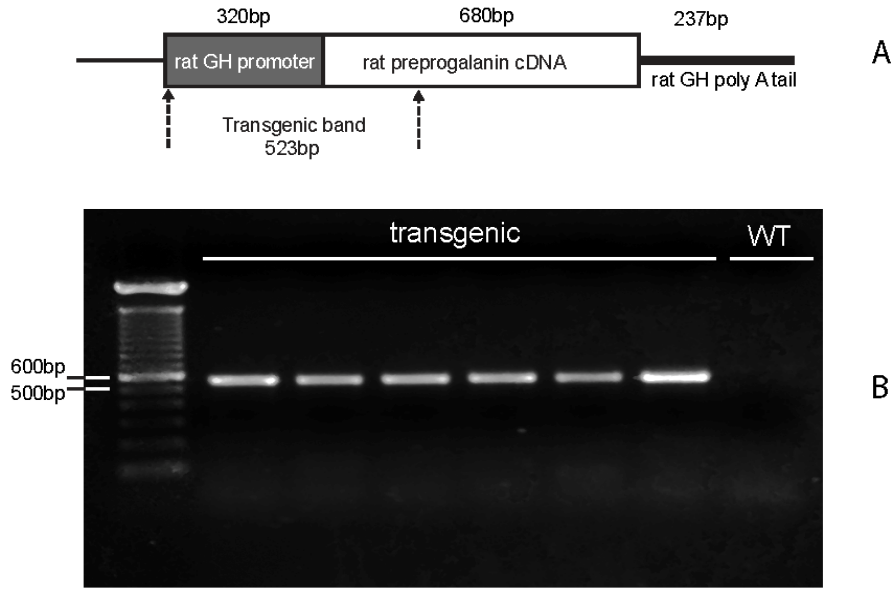

Figure 1 Schematic structure of the transgene and representative genotyping PCR (A) The diagram showing the constructed galanin transgene. Dr.Vrontakis, et al. designed the transgene by fusing the 320 bp-length KpnI/XhoI fragment of the rat GH promoter to a full-length rat preprogalanin cDNA followed by the 237 bp-length poly A tail of the rat GH gene (Perumal, 2003). (B) A representative genotyping result. By using the GH upper and Gal lower primers, described in the Materials and Methods section, a band of 523 bp was amplified by polymerase chain reaction, indicating the positive genotyping results, while in the wild-type mouse, the band could not be detected. The schematic structure of the transgene is created by Adobe Illustrator CS4.

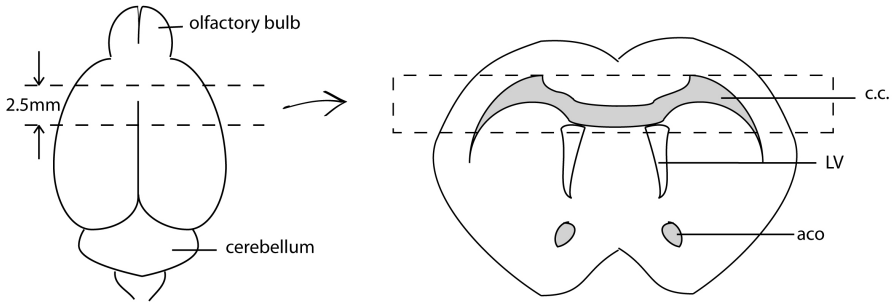

Figure 2 The source of RNA samples. The illustration on the left demonstrates the mouse brain. The dashed line above was the first coronal cut 5 mm away from the edge of the olfactory bulb, and the dashed line below was the second coronal cut 2.5 mm away from the first cut. The diagram on the right is the brain section obtained from the cuts shown on the left. The tissue within the dashed rectangle, which mainly contains corpus callosum and part of the cortex, was used for RNA extraction for the detection of gene expression in the CC. Abbr.: CC Corpus callosum; LV, lateral ventricle; aco, anteriorcommissure/olfactory limb

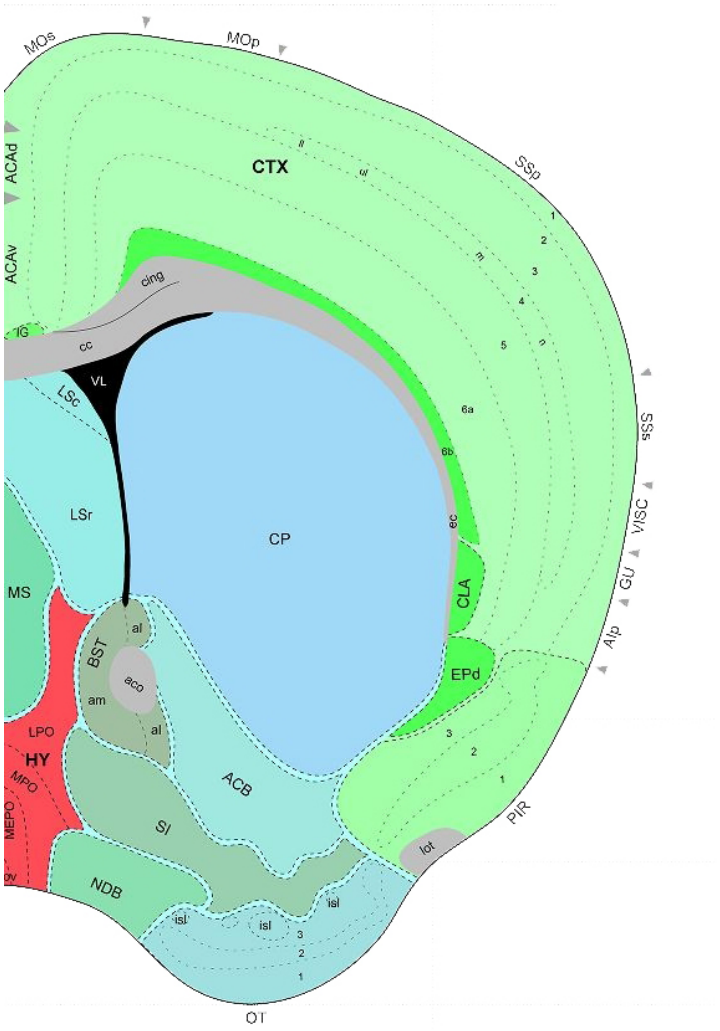

Figure 3 Allen mouse brain atlas Downloaded from The Allen Institute for Brain Science website (http://mouse.brain-map.org/viewImage.do?imageId=130962). The usage of the atlas followed the Citation Policy detailed by Allen Institute (http://www.alleninstitute.org/about_us/citation_policy.html). The presenting illustration at coronal level 49 was used as the main reference brain section throughout the study. The coronal level is determined according to the Allen mouse reference atlas. Abbrev. cc, corpus callosum; CTX, cortex; ec, external capsule (of cc); cing, cingulum bundle; PIR, piriform area; aco, anterior commissure/olfactory limb; VL, lateral ventricle; HY, Hypothalamus; CP, caudoputamen

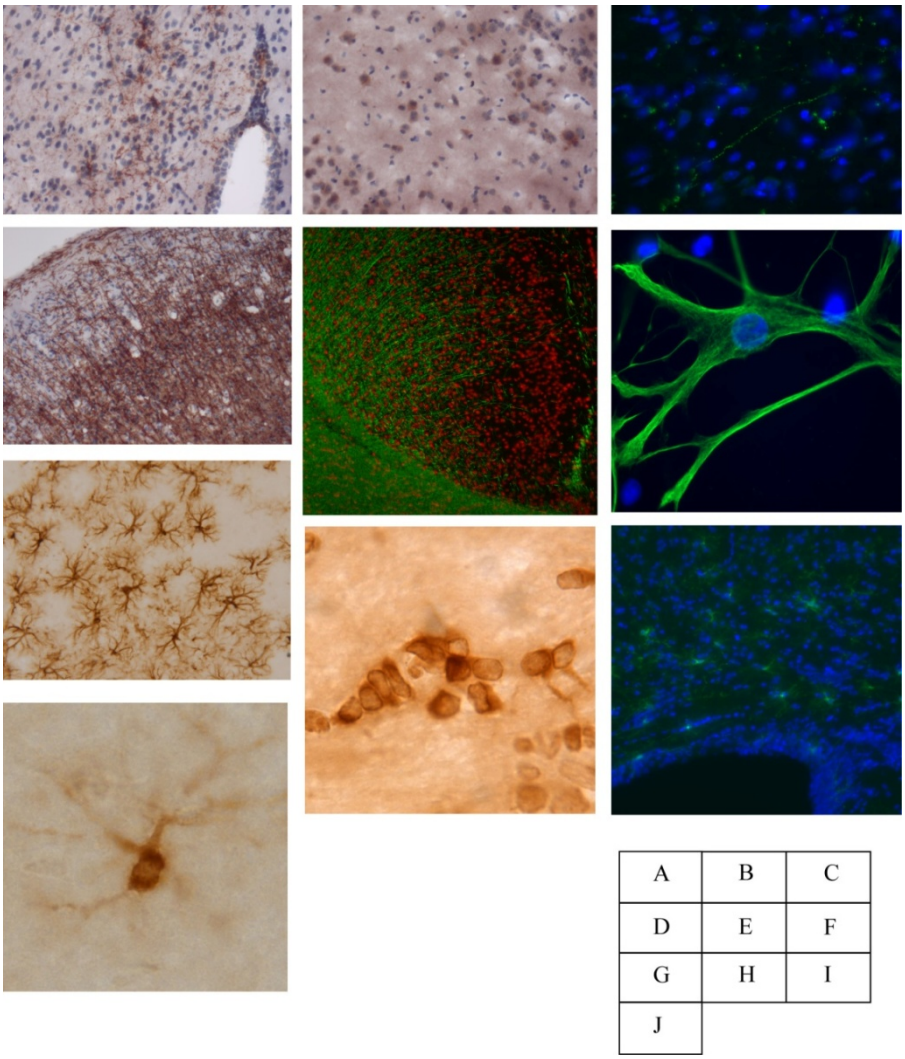

A	B	C
D	E	F
G	H	I
J		

Figure 4 Representative images of immunostaining (A) Immunohistochemistry (IHC) using the galanin antibody (under 20x lens). The image was taken at the site of the hypothalamus where fiber-like staining could be observed. (B) The same sample as in (A), but the image was captured at the site of the piriform area where galanin was presented in the cytoplasm of some neuron-like cells. (C)Immunofluorescence (IF) of galanin (Galanin/Hoechst 33342, under 60x lens). The area was from the hypothalamus. (D) IHC of MBP (under 10x lens) showing fine fibers of myelin in the cortex. (E) IF of MBP (MBP/Hoechst 33342, under 20x lens) showing fine fibers of myelin in the cortex and condensed staining in the CC. (F) IF of astrocyte cell culture using GFAP antibody (GFAP/Hoechst 33342, under 1,000x lens), demonstrating the skeletal structure of GFAP inside the cell body. (G) IHC of the mouse brain using GFAP antibody (under 40x lens). The image was taken at the site in the cortex of a mouse from the demyelination group. (H) IHC of GST-π showing mature oligodendrocytes presented in CC in linear (under 1,000x lens). (I) IF of PDGFR-α in CC (PDGFR-α/Hoechst 33342, under 20x lens). (J) IHC of PDGFR-α in the cortex (under 1,000x lens).

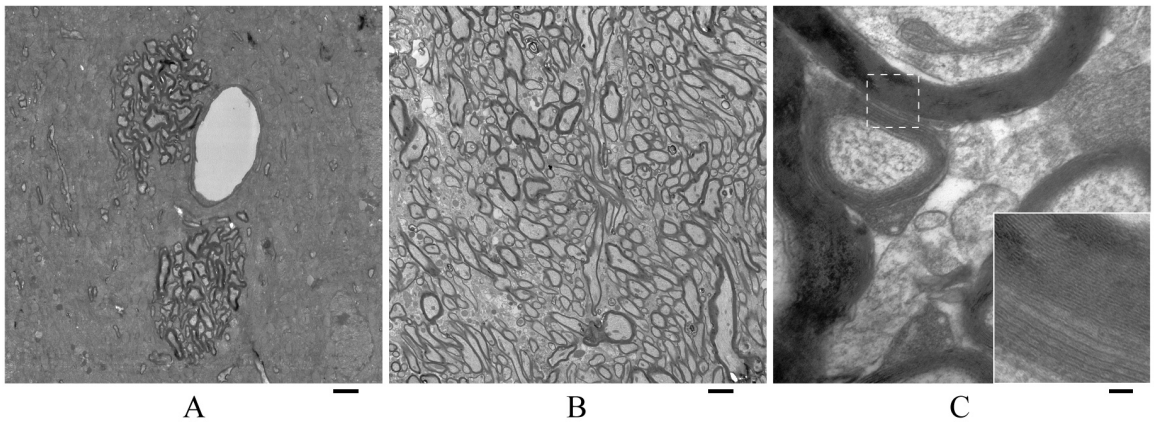

Figure 5 Transmission electron micrograph of myelinated fibers in a transverse section (A) Two bundles of myelinated axons and an adjacent blood vessel in the cortex of the mouse brain. The magnification was 3,400x (B) An image of a CC area showing compact clusters of myelinated fibers with different diameters and different thicknesses of myelin sheaths at a magnification of 3,400x. (C) High magnification of myelinated axons. Axons were wrapped by the multiple layers of myelin lamellae. In graph (C), a further magnified graph showing the detail multiple-membrane lamellae was took from the dashed rectangle area. The magnification of (C) was 64,000x. The scale bars below (A) and (B) represented 500 nm, while the one below (C) equaled a length of 100 nm.

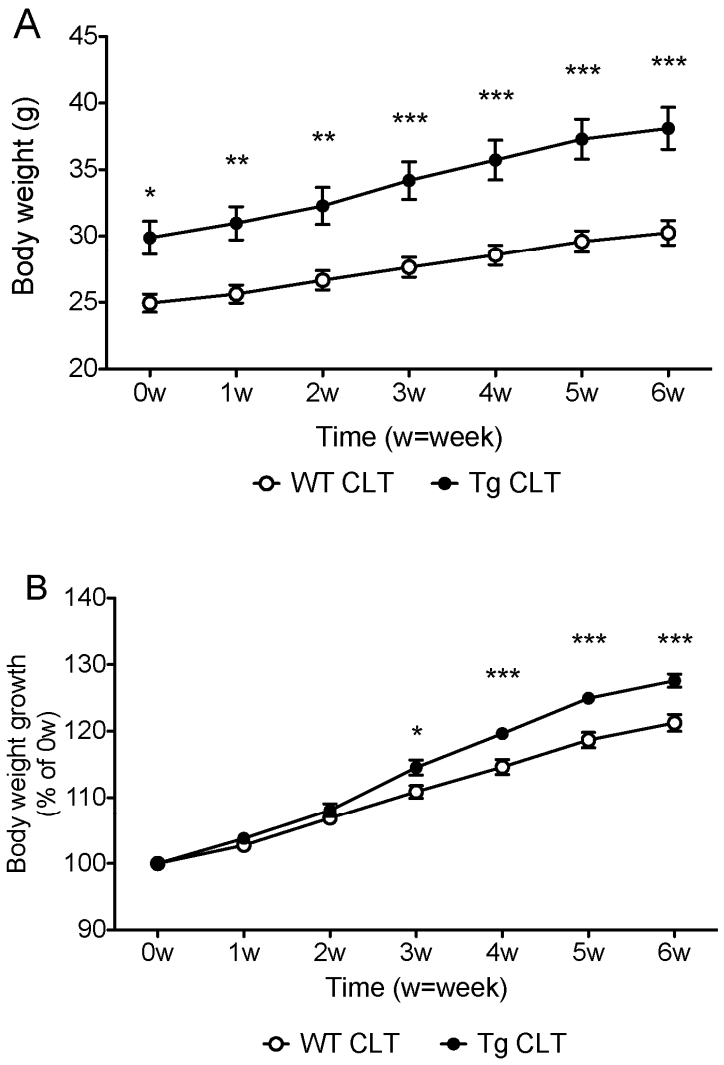

Figure 6 Body weight growth of unchallenged mice Body weight was measured at the age of 8~9 weeks old as the starting point as 0 w. (A) The raw body weight of both WT and Tg mice. (B) The rates of body weight growth are presented as the percentage of gained body weight compared to the initial body weight. Data are expressed as the means±s.e.m. (n=12~17 per group). * $p<0.05$ ** $p<0.01$ *** $p<0.001$

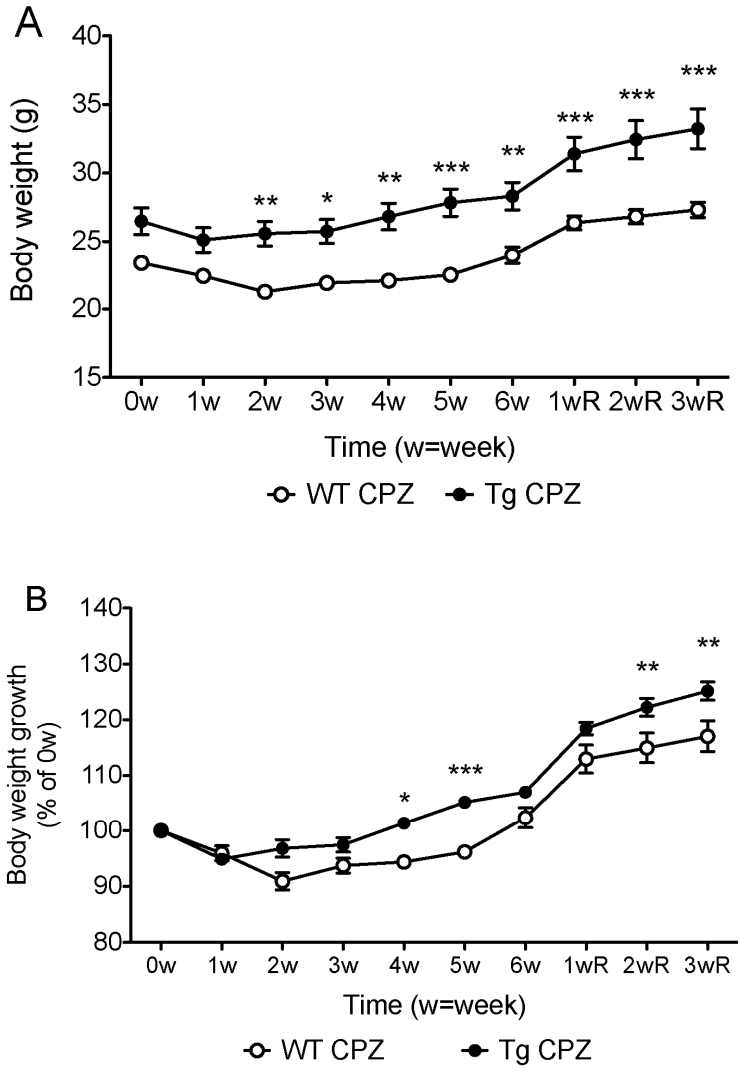

Figure 7 Body weight growth of CPZ challenged mice. Body weight was measured beginning at the age of 8~9 weeks old as the starting point as 0w. After six weeks of CPZ challenge, mice were allowed to recover for an additional three weeks as 1wR, 2wR and 3wR. (A) The raw body weight of both WT and Tg mice in CPZ-induced challenge groups. (B) The rates of body weight changes are presented as the percentages of changed body weights compared to the initial body weights. Data are expressed as the means±s.e.m. (n=12~17 per group). * $p<0.05$ ** $p<0.01$ ***$p<0.001$

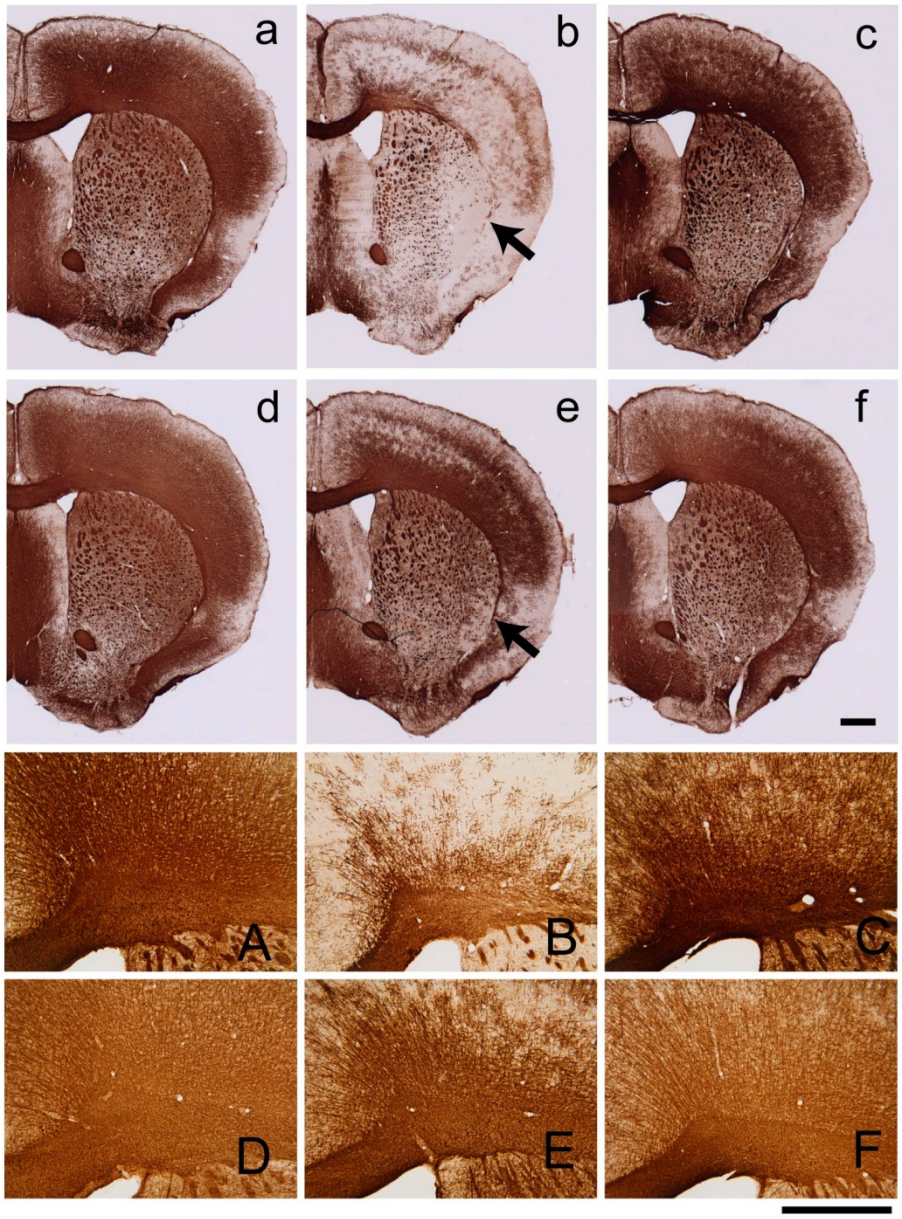

Figure 8 Increased galanin reduced CPZ-induced myelin breakdown Myelin was detected by IHC using an MBP antibody at a dilution 1:500. Images were visualized by DAB color development. (a~f) shows the images of the whole brain staining, while (A~F) are images of the knee part of the cc under higher magnification. (a),(b) and (c) are representative images of WT control mice, WT 6wCPZ mice and WT 6wCPZ+3wR mice, respectively, while (d), (e) and (f) demonstrate the same groups in Tg mice. The arrows in (b) and (e) are pointing at the external capsule of corpus callosum. The scale bars are both 500 μm.

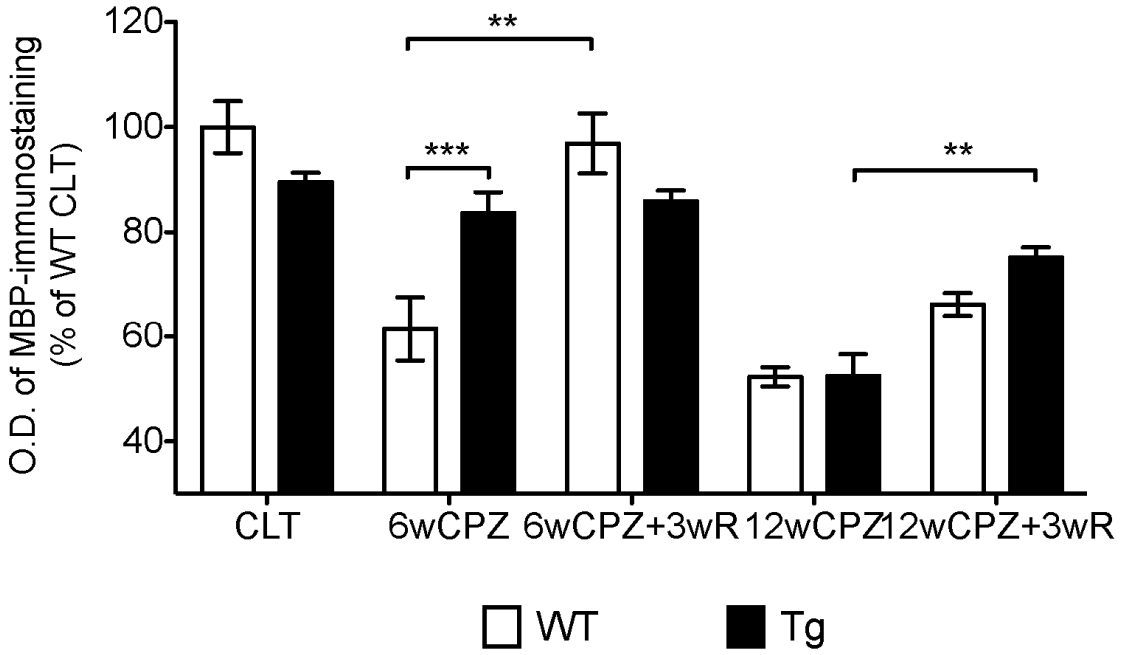

Figure 9 The relative optical density (O.D.) of MBP staining. The bar chart of O.D. measurements of MBP staining. The mean of WT CLT O.D. values was used as the relative value that was 100%. The remaining O.D. relative values were calculated according the mean value of WT CLT. Data are expressed as the means ± s.e.m. (n = 6/group). ***p<0.001 between WT and Tg mice in 6wCPZ groups. **p< 0.01 between the WT mice in 6wCPZ group and the 6wCPZ recovery group compared to the CNT group. **p< 0.01 between Tg mice in 12wCPZ group and 12wCPZ recovery group.

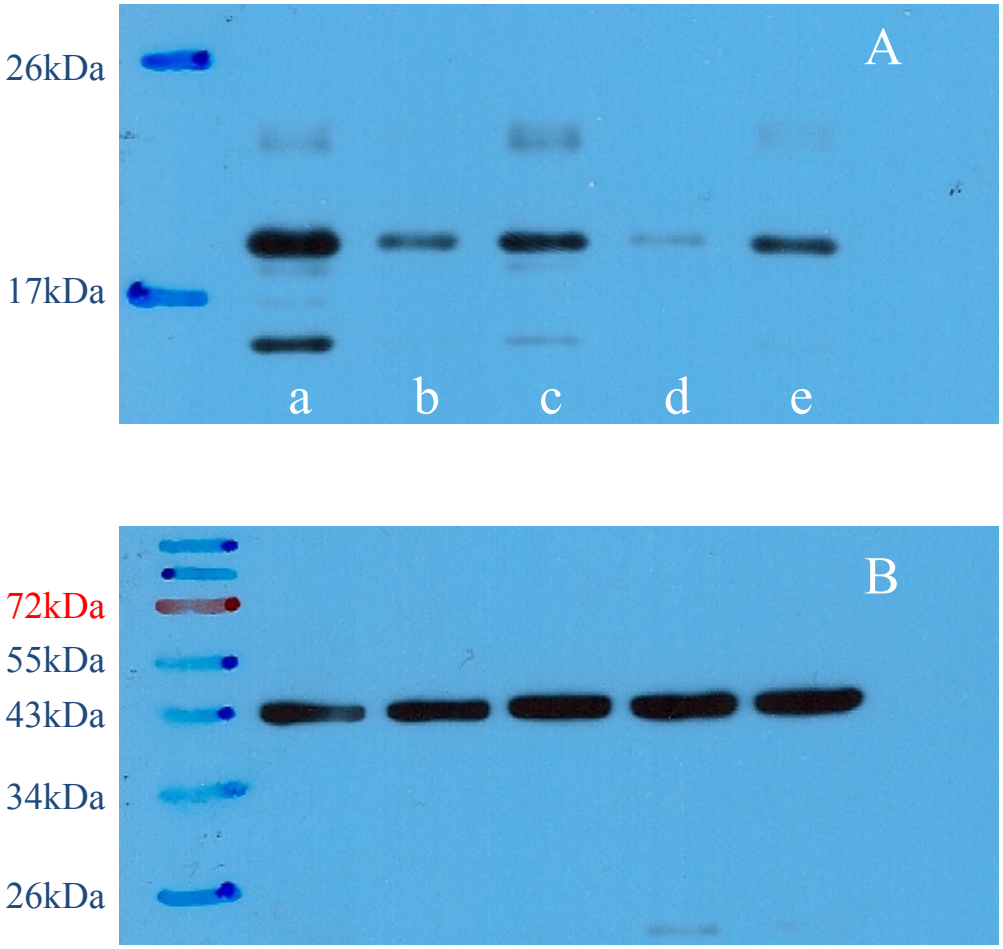

Figure 10 Western-blot analysis of MBP and beta-actin in WT mice Films (A) and (B) show the western blotting of MBP protein and beta-actin protein, respectively. In (A), the bands of a, b, c, d, and e represent the protein samples from control group (CLT), six-week CPZ challenge group (6wCPZ), six-week CPZ challenge recovery group (6wCPZ+3wR), twelve-week CPZ challenge group (12wCPZ), and twelve-week CPZ challenge recovery group (12wCPZ+3wR), respectively.

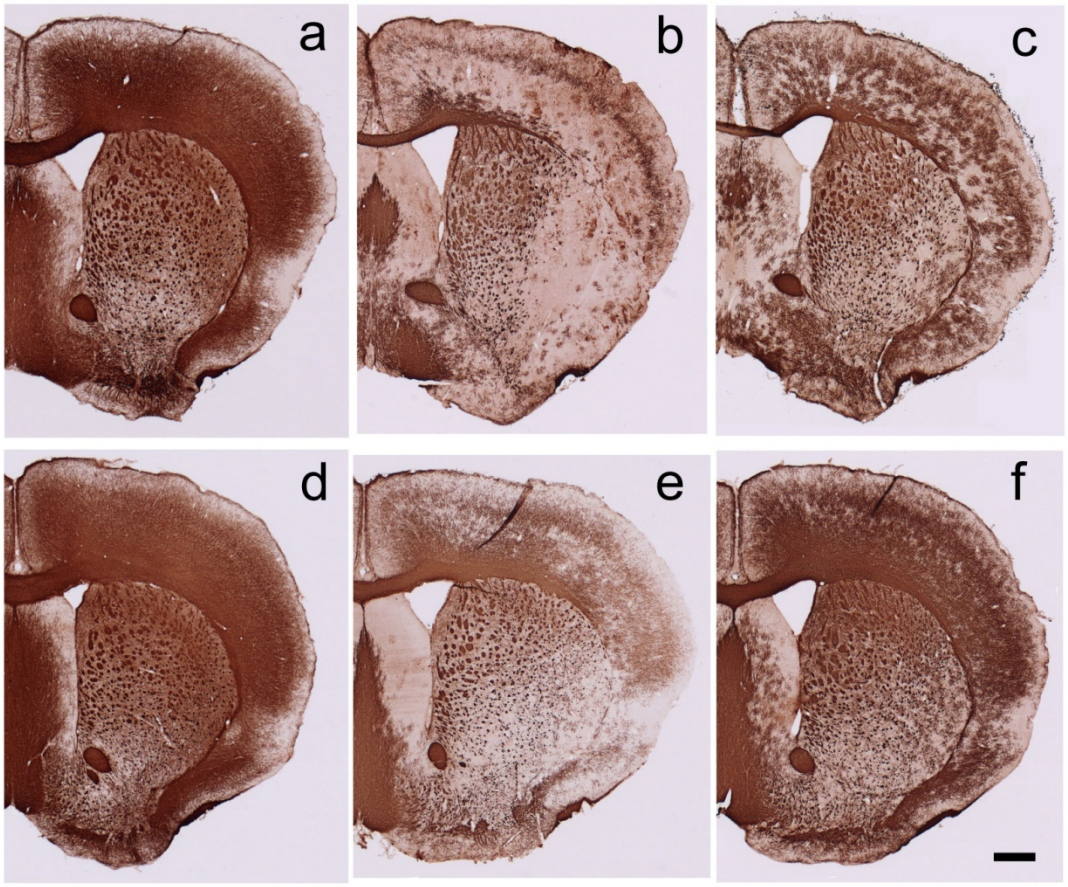

Figure 11 Increased galanin promotes re-myelination after the prolonged CPZ-induced demyelination Myelin was detected with IHC using an MBP antibody at a dilution of 1:500. The images were visualized by DAB color development. (a),(b) and (c) are the representative images of WT control mice, WT 12wCPZ mice and WT 12wCPZ+3wR mice, respectively, while (d), (e) and (f) demonstrate the same groups in Tg mice. The scale bar is 500 μm.

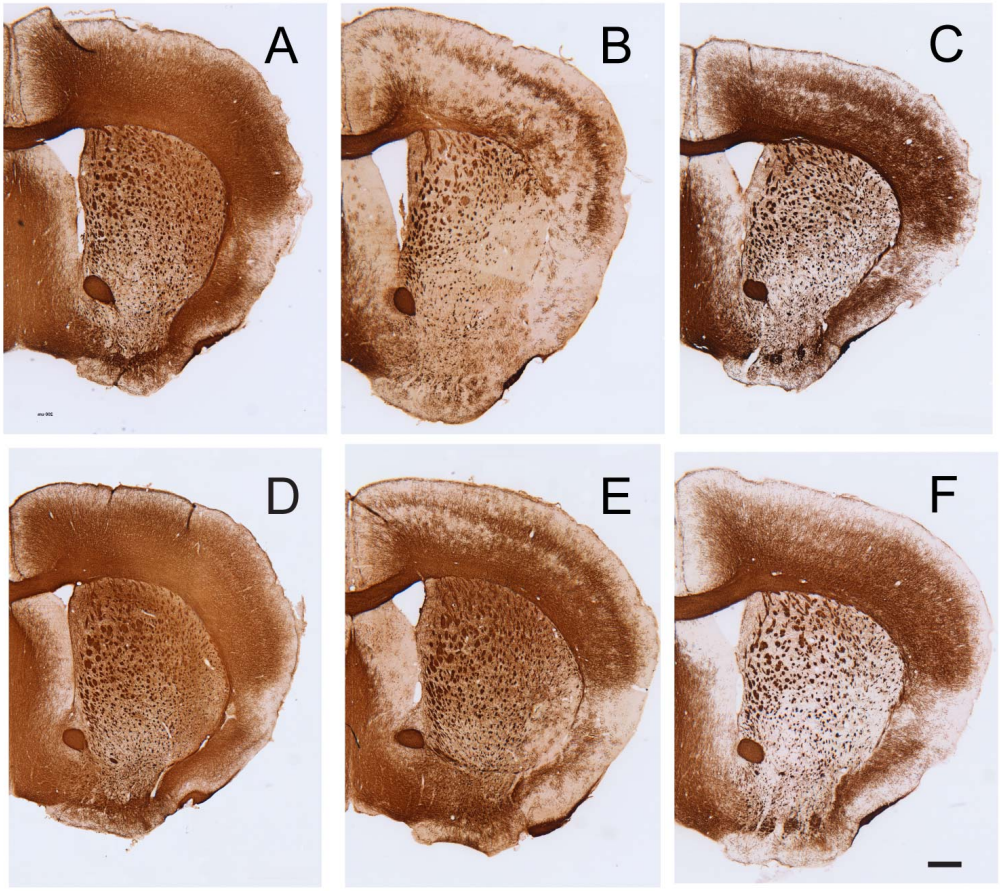

Figure 12 Administration of estrogen alleviates CPZ-induced myelin breakdown Myelin was detected by IHC using an MBP antibody at a dilution of 1:500. The images were visualized using DAB color development. (A),(B) and (C) are the representative images of WT control mice, WT 6wCPZ mice and WT E3+6wCPZ mice, respectively, while (D), (E) and (F) demonstrate the same groups in Tg mice. The scale bar is 500 μm.

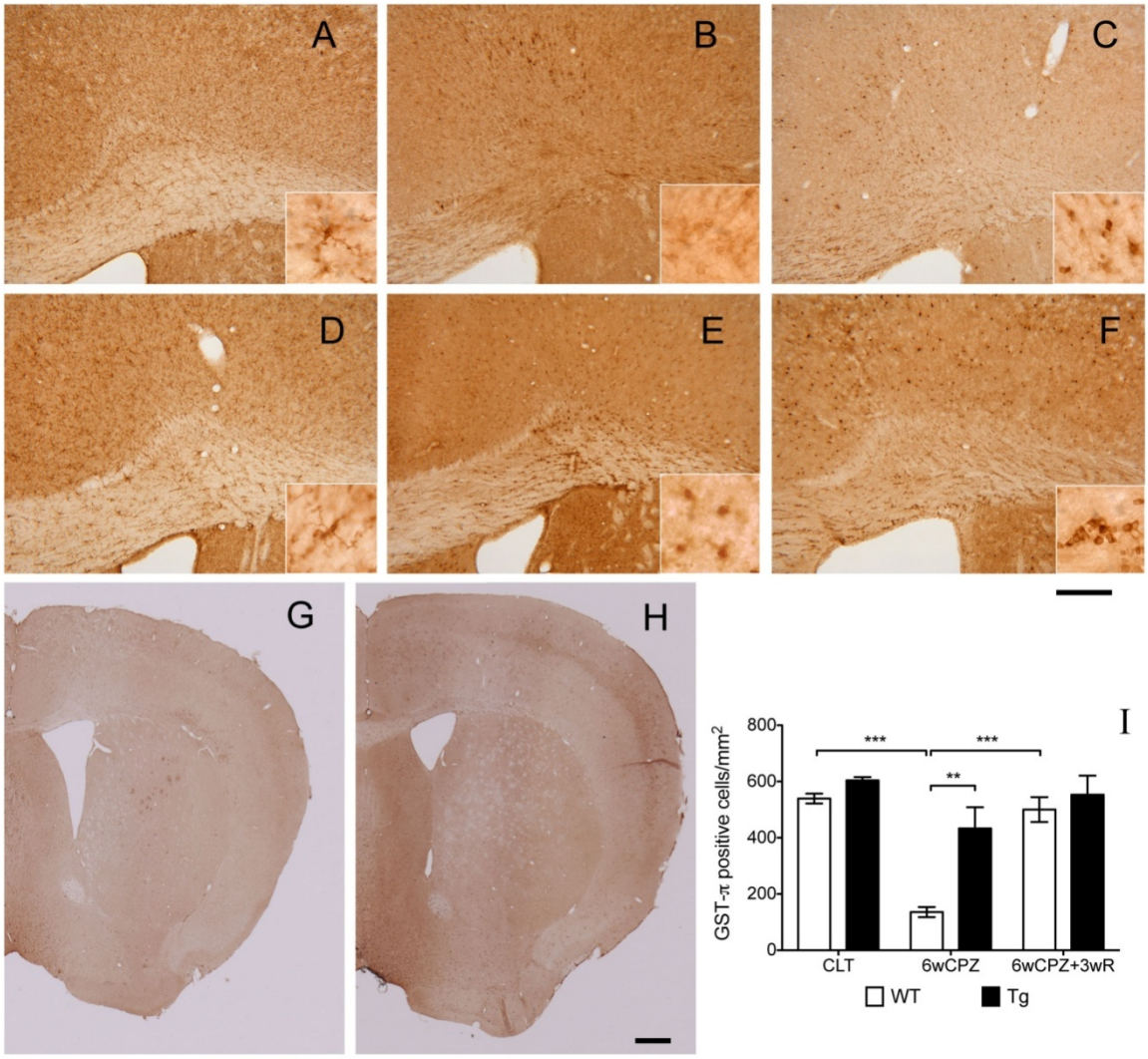

Figure 13 Increased galanin reduces CPZ-induced death of oligodendrocytes. Mature oligodendrocytes were detected with IHC using a GST-π antibody. (A~F) were taken from the knee region of the CC, and (G) (H) were the whole pictures of WT and Tg from the 6wCPZ group. The three CC images in the upper panel show the WT mice in CTL, 6wCPZ and 6wCPZ+3wR groups, and the images in the lower panel show the Tg mice in the same groups. In (A~F), high magnification micrographs were taken from the CC area under an oil lens, as demonstrated in the dashed rectangle inserts. (I) Bar chart displays the numbers of GST-π positive cells counted manually. **p<0.01, ***p<0.001, n=3 in each group. The longer bar represents a length of 200 μm, and the short bar represents 500 μm.

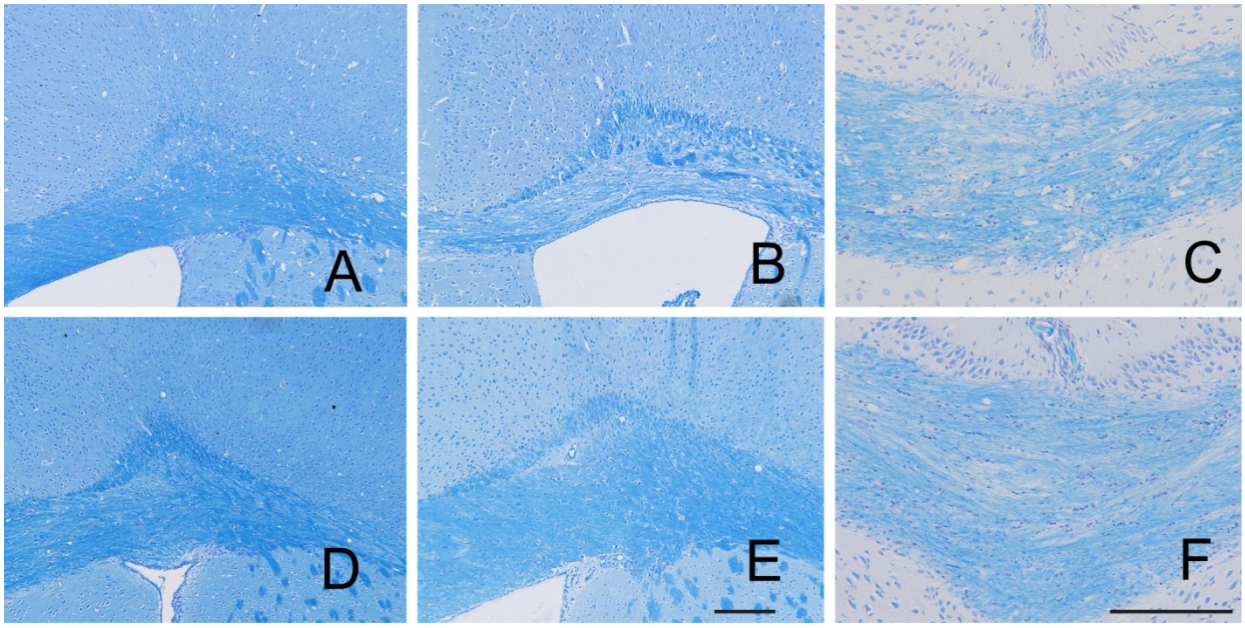

Figure 14 Luxol fast blue staining (A) and (B) are the stained images of brains from WT CLT and WT 6wCPZ groups respectively, while (D) (E) are the images of Tg mice from the same manipulation groups (under 10x lens). (C) and (F) show the center area of the CC from WT 6wCPZ group and Tg 6wCPZ group respectively at higher magnification (under 20x lens). Both scale bars indicate a length of 200 μm.

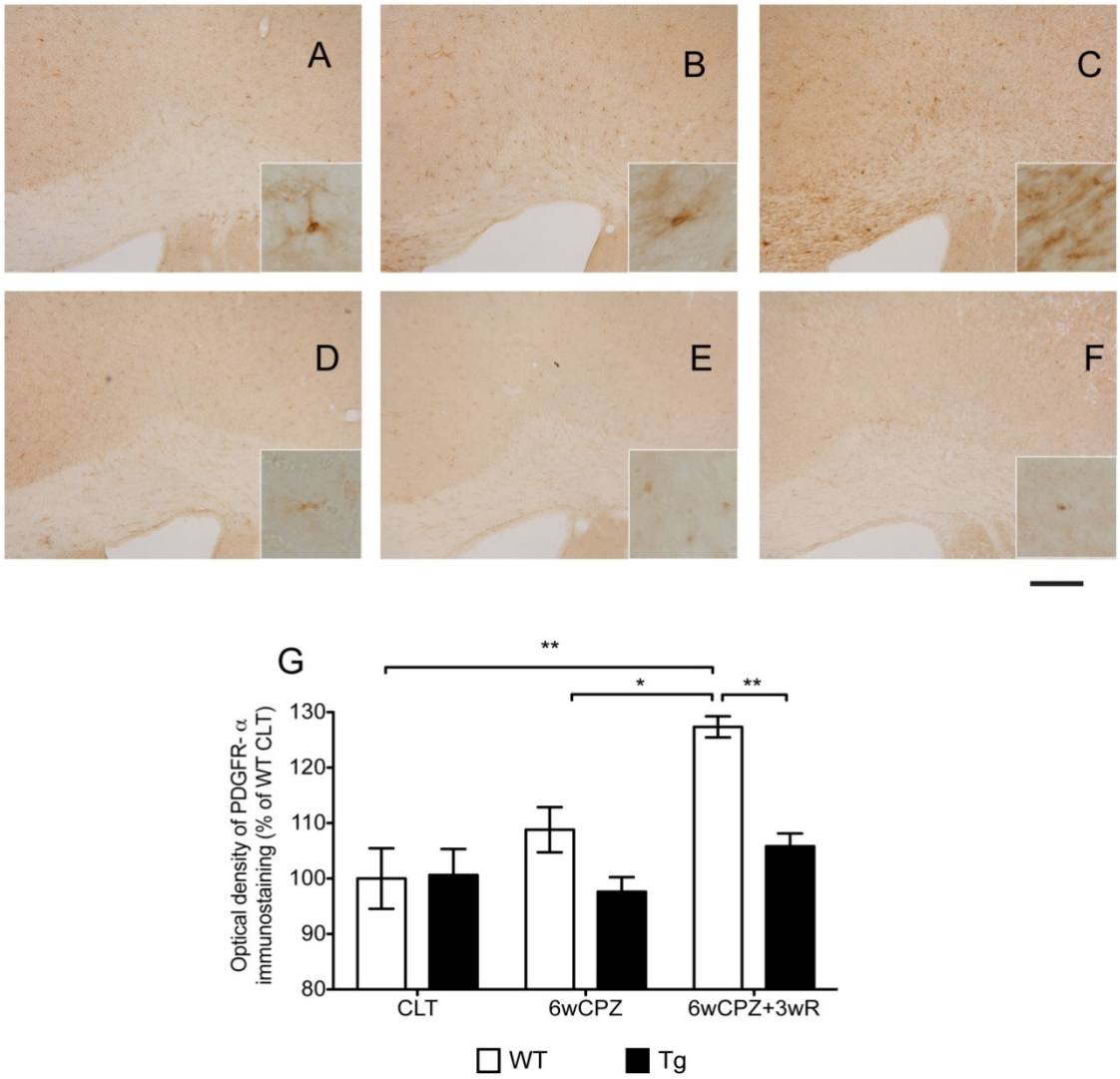

Figure 15 Elevated galanin suppresses the CPZ-induced PDGFR-α positive immunostaining. (A)~(C) contains images of WT mice from CLT, 6wCPZ and 6wCPZ+3wR groups, and (D)~(F) shows the Tg mice from the same groups in the corresponding order to (A)~(C). (G) is a bar chart of O.D. measurements of PDGFR-αstaining. The mean of WT CLT O.D. values were used as the relative value that was 100%. Data are expressed as the means ± s.e.m. (n = 3 per group). *p<0.05 **p<0.01, the scale bar equals 200 μm.

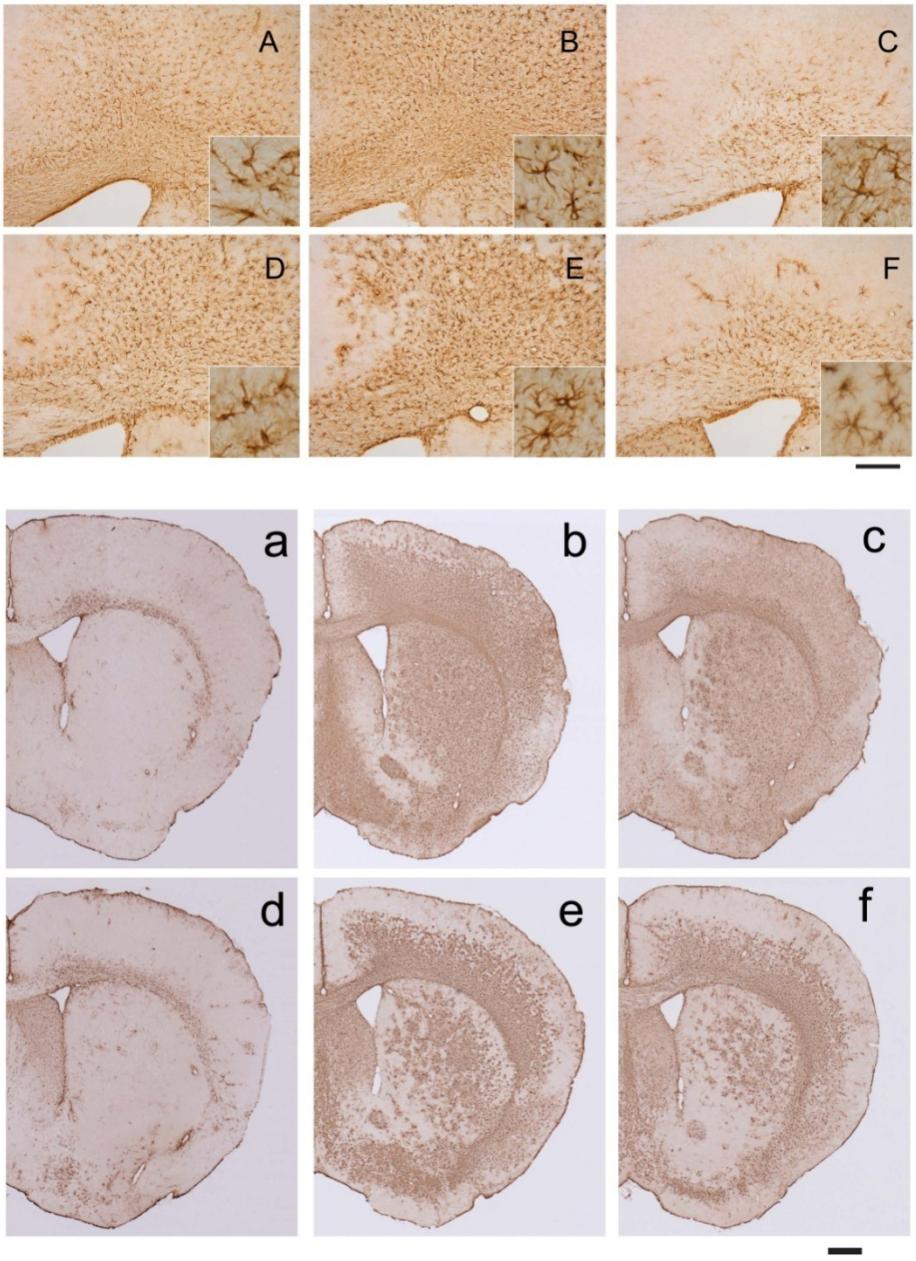

Figure 16 Over-expressed galanin restricts reactive astrogliosis Reactive astrogliosis is defined as a response to brain injury where astrocytes undergo hypertrophy and proliferation. In this study, astrocytes were detected by IHC using a GFAP antibody at a dilution of 1:1000. The images were visualized by DAB color development. (a~f) shows the images of whole brain staining, while (A~F) are images of the knee part of the CC under higher magnification. (a), (b) and (c) are representative images of WT control mice, WT 6wCPZ mice and WT 6wCPZ+3wR mice, respectively, while (d), (e) and (f) demonstrate the same groups in Tg mice. The scale bars are 200 μm for (A~F) and 500 μm for (a~f).

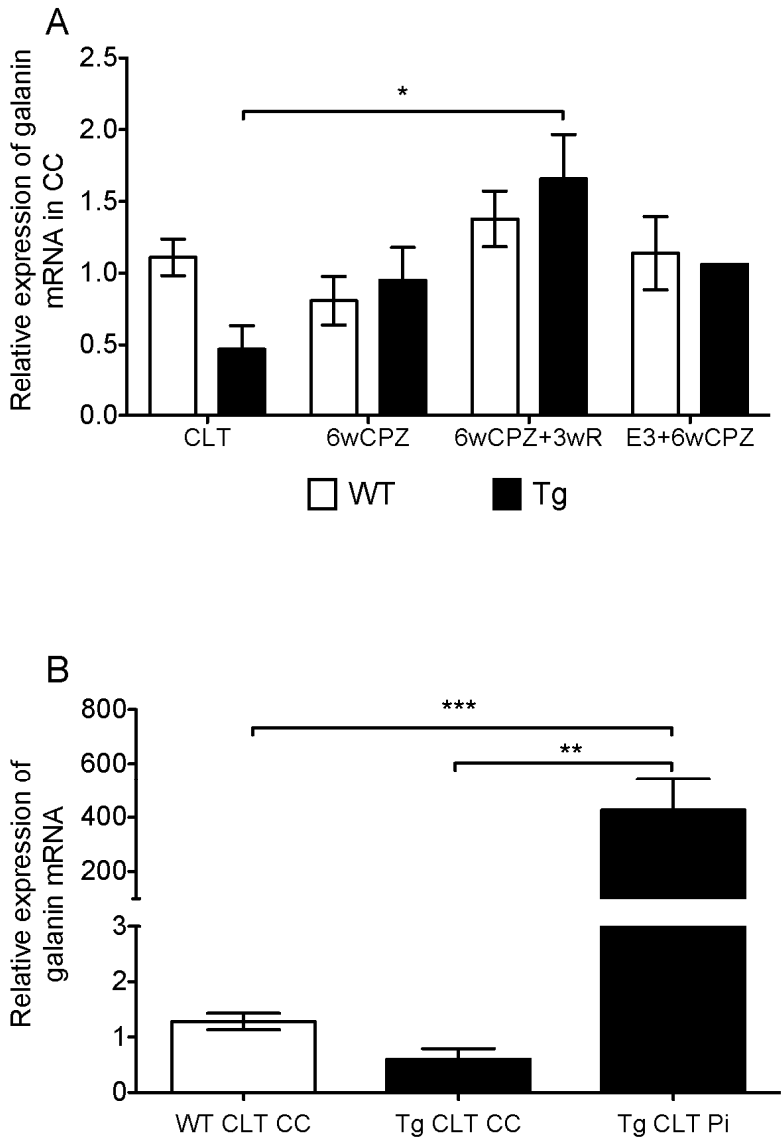

Figure 17 Relative expression of Galanin mRNA Expression of galanin mRNA was measured using real-time PCR. Total RNA samples were subjected to quantitative real-time PCR as described in the Materials and Methods section. The expression of galanin mRNA relative to the level of GAPDH is shown. Results are expressed relative to WT control mice that were standardized to the value of 1. (A) shows galanin expression in the CC, and (B) demonstrates the comparison of galanin expression levels under the normal unchallenged condition among pituitary (Pi) in Tg mouse, CC in Tg mice and CC in WT mice. The group Tg E3+6wCPZ group only contained one mouse where there were no error bars in (A) and n=2 in Tg CLT pi group in (B), while the sample sizes of the rest of the groups were 3~4 per group, $*p< 0.05$, $**p<0.01$ $***p<0.001$

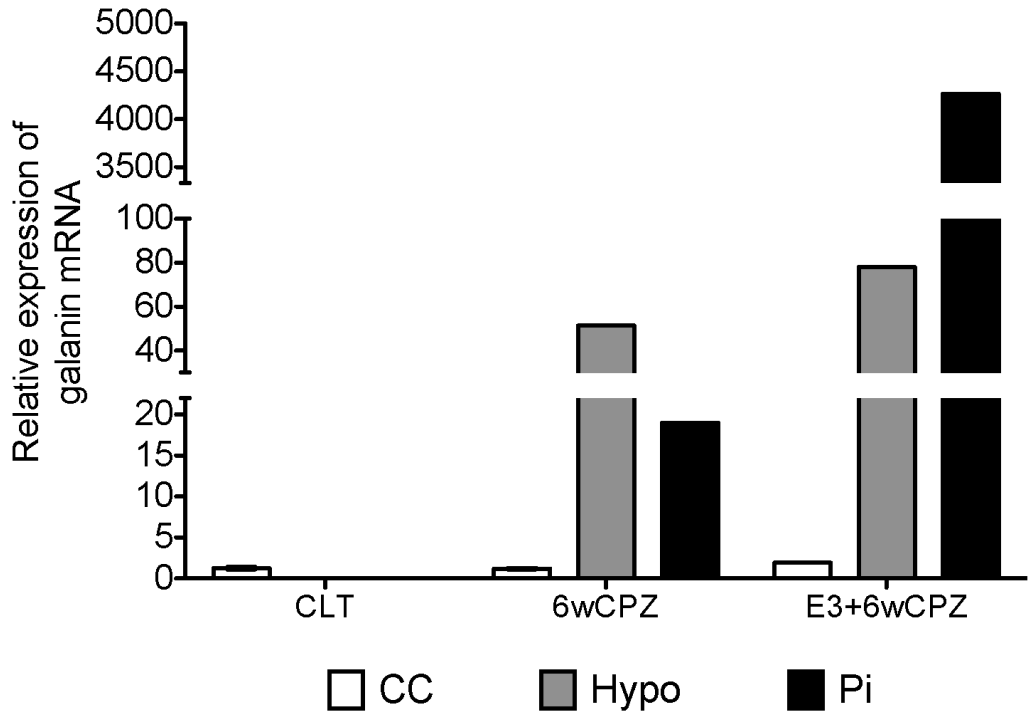

Figure 18 Differential expression of Galanin mRNA in WT mice. The expression of galanin mRNA was measured by real-time PCR. Total RNA samples were subjected to quantitative real-time PCR as described in the Materials and Methods section. The expression of galanin mRNA relative to the level of GAPDH is presented. Results are expressed relative to WT control mice that were standardized to a value of 1. The chart demonstrates the expression levels in the corpus callosum (CC), hypothalamus (Hypo) and pituitary (Pi) under the conditions of normal control (CLT), semi-acute six weeks CPZ challenge (6wCPZ) and six weeks CPZ challenge combined with the treatment of estrogen (E3+6wCPZ). There was only one hypo and pi sample in each group and one cc sample in E3+6wCPZ group, thus there are no error bars, while there were four CC samples in CLT and 6wCPZ group. Due to the size of the sample, statistical analysis was not available.

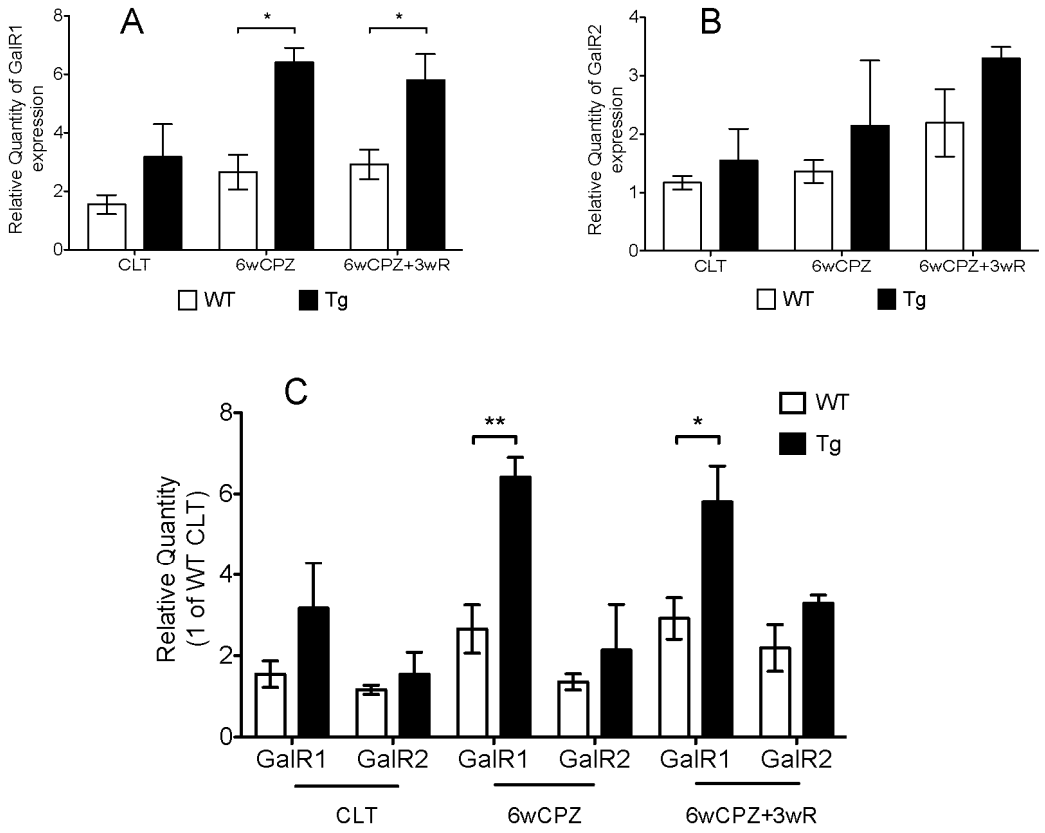

Figure 19 The relative expression of GalR1 and GalR2 in the CC. The expression of GalR1 and GalR2 was detected using real-time PCR. The expression of GalR1 and GalR2 mRNA relative to the level of GAPDH is presented. Results are expressed relative to one reference mouse in WT control group (WT CLT) that was standardized to a value of 1. (A) is the diagram of expression levels of GalR1 in the CC, and (B) is the chart of GalR2 expression in the CC. (C) was generated by combining data from (A) and (B), and the expression of GalR1 in the same reference animal in WTCLT was used as the reference value of 1.

CHAPTER 6: DISCUSSION AND CONCLUSIONS

GAL has diverse biological functions in the nervous system. The traditional view of GAL's biological functions were intensively focused on its regulation effects as a hypothalamic neuropeptide. The predominant observation was its effects on feeding. Administration of GAL directly into the paraventricular nucleus in Hypo in rat was found to increase the food intake in a dose-dependent manner (Bartfai et al., 1993; Walton et al., 2006). Because GAL co-exists with many other classical neuropeptides such as GABA, enkephalin, substance P and neuropeptide Y(Simmons et al., 1995), the regulation effects of GAL together with those neuropeptides on other functions were also reported such as the roles in cognitive functions including learning and memory, in affective processes including depression and anxiety, in sleep, and in pain (Rodriguez Diaz et al., 2011; Szymusiak et al., 2007; Vrontakis, 2002; Werner and Covenas, 2010). Moreover, recently GAL has been found to have neuroprotective and neurotrophic functions on neurons in the nervous system (Bartfai et al., 2004; Hobson et al., 2008; Lee et al., 2005; Walton et al., 2006).

Besides the functions of GAL on neuron, a potential involvement in myelin development had been demonstrated previously by Shen, et al. (Shen et al., 2005). Although the pathways for the protective and trophic effects of GAL are not yet clear, the present project may reveal the direct participation of GAL in myelin protection and promotion against CPZ-induced demyelination and during the re-myelination phase. Furthermore, the differential stimulation of GAL in Hypo and Pi by estrogen may indicate that the GAL pathway is one of the mechanisms for the neuroprotective function of this pregnancy hormone of E3. The gene expression studies also found the potential

involvements of GalR1 and GalR2 in the protective roles of GAL differentially in the demyelination and re-myelination phases. Uniquely, unlike other GAL transgenic models (Bacon et al., 2002; Crawley et al., 2002), the circulating levels of GAL in these Tg mice were 10-fold higher than in WT mice (Perumal and Vrontakis, 2003), and the high expression of GAL in the Pi in these Tg mice was further confirmed in this project using real-time PCR. This advantage allows the Tg mice to receive a more consistent source of GAL from the peripheral circulation. The neuroprotective effect from the high level of circulating GAL might further indicate the potential utility of GAL by an intravenous drip infusion instead of intracerebroventricular administration.

6.1. The neuroprotective effects of GAL

GAL is a biologically active neuropeptide that is widely distributed in the CNS in all mammals studied. One of the essential characteristics of this neuropeptide is its plasticity, in that its expression can be dramatically up-regulated or down-regulated by various stimuli in different tissues, as demonstrated by previous studies (Beal et al., 1990; Villar et al., 1989; Vrontakis et al., 1989). Importantly, more recent studies have revealed that this highly inducible peptide has a novel protective and trophic effect on neurons in the CNS mainly through the activation of GalR2 (Ding et al., 2006; Elliott-Hunt et al., 2004; Elliott-Hunt et al., 2007; Hobson et al., 2008; Mahoney et al., 2003; Mazarati et al., 2004). In comparison, the role for GAL in myelinogenesis is still relatively new. Despite some trial experiments that attempted to link GAL and myelination, studies of the roles of GAL in glial cells and myelination are not well developed.

In this project, using a GAL over-expressing transgenic mouse, we found a novel attenuation of oligodendrocytes and myelin against the CPZ-induced demyelination in terms of a reduction in the death of mature oligodendrocytes and an alleviation in myelin breakdown in GAL Tg mice. Myelin basic protein (MBP) is a structural protein of the myelin sheath. Furthermore, MBP is believed to be a vitally important functional protein for myelin assembly and maintenance. MBP IHC staining, which was applied in the present study, is commonly used for quantitatively detecting the myelin sheath (Chekhonin et al., 2000). Thus, after a six-week exposure of CPZ challenge, the significant loss of MBP staining in WT mice could be considered to be a severe demyelination, and the attenuated MBP staining results in Tg mice suggest an alleviated demyelination. In addition, the DAB-dye-based IHC staining results were further verified by Luxol Fast Blue staining, another histological myelin staining method commonly used by other researchers. Furthermore, the loss of MBP protein in WT mice was further tested using the western blotting with the same antibody applied for IHC staining. Overall, these data supported our findings that the alleviated demyelination in Tg mice was repeatable and reliable.

Interestingly, despite the severe demyelination in the WT mice after six weeks of CPZ exposure, a layer of MBP staining remains intact in the cerebral cortex. Through comparison with the reference mouse brain atlases (Fig. 3), we found that this layer contains the somato-sensory neurons. Although we do not have direct evidence showing that the protective effect on this layer of myelin is related to the effect of GAL, it is well known that GAL is involved in neuropathic pain and that the GAL peptide is dramatically increased in the sensory neurons and dorsal root ganglia after pathological challenge

(Holmes et al., 2000; Wiesenfeld-Hallin and Xu, 1998). This observation warrants further study.

Because the experimental demyelination induced by CPZ is based on the apoptosis of oligodendrocytes (Matsushima and Morell, 2001), we next examined the number of mature OL in the different groups. GST-π is a myelin- and oligodendrocyte-associated enzyme in the brain that is used as a biomarker for mature oligodendrocytes (Tansey and Cammer, 1991). We found that, in terms of CPZ-induced demyelination, the degradation of GST-π positive cells seen in WT mice was greatly alleviated in our Tg mice. In this study, we also found that the OPCs were highly proliferative and accumulated in response to CPZ-induced OL degradation in the WT mice, while in Tg mice, the response was minimal. Additionally, the detection results of OPCs were supported by the observations of the survival of mature oligodendrocytes, as revealed by GST-π staining. It had been suggested that the infiltrating proliferative OPCs were recruited to reverse the loss of the mature oligodendrocytes by proliferating and then differentiating into mature oligodendrocytes, and the OL death in the lesions can be characterized by a repopulation of OPCs prior to new OL formation (Miron et al., 2011). These findings supported the hypothesis that low proliferation and accumulation of OPCs in Tg mice are due to the improvement of oligodendrocytes survival.

It is well known that, in the CPZ treated mouse, demyelination is accompanied by reactive astrogliosis. Similar to those early studies (Groebe et al., 2009; Kipp et al., 2009; Matsushima and Morell, 2001), we also found widespread invasions of reactive astrogliosis in WT mouse brains following six weeks of CPZ exposure. However, in our Tg mice after the same challenge, the reactive astrogliosis was limited to a more narrow

area in the cortex that did not extend beyond cortical layer four. Although further investigations are needed to reveal the mechanisms in the limited diffusion of reactive astrogliosis in the cerebral cortex of Tg mice, the suppressed reactive astrogliosis strongly suggests that the demyelination were limited in terms of the decreased reaction of astrogliosis in GAL Tg mice.

Besides the protective effect against the six weeks of CPZ-induced semi-acute demyelination, the over-expression of GAL promoted the regeneration of myelin following chronic demyelination. As revealed by the early studies of the CPZ model, the endogenous re-myelination ability in WT mice is still strong after six weeks of CPZ-induced demyelination, thus even though the over-expression of GAL promoted re-myelination after semi-acute demyelination, the observation window was too narrow to determine a difference between WT mice and Tg mice. Based on the observation that as demyelination becomes prolonged the native re-myelination ability becomes weak (Matsushima and Morell, 2001), we suppressed the native re-myelination ability by challenging both WT and Tg mice with a twelve-week CPZ-induced chronic demyelination. The recovery results indicated that, although the both genotypes of mice showed severe demyelination after the chronic challenge, a three-week recovery was sufficient to observe a difference between WT mice and Tg mice in the re-myelination ability. Besides MBP staining, we do not currently have other direct evidence to investigate the mechanisms of over-expressed GAL on the promotion of re-myelination; however the high lipid metabolism and the neurotrophic effects of GAL are potentially involved.

It has been well accepted that GAL acts through three G-protein-coupled receptors, GalR1, GalR2 and GalR3, and that these three receptors activate distinct G-proteins that participate in different GalR-signaling pathways and result in diverse biological functions upon the binding of GAL or other ligands (Branchek et al., 2000). In this study, a gene expression assay revealed that the expressions of GalR1 and GalR2 was differentially altered in the demyelination and re-myelination phases indicating their differential involvements during those two phases; the reaction of GalR1 in the initial challenge phase may due to its protective effect in the response of the demyelination, while the up-regulation of GalR2 in the later recovery phase may indicate a neurotrophic effect for the recovery. However, the gene expression assay in this study could not provide direct evidence to the mechanisms of those two receptors in the de-myelination and the re-myelination. Studies on their mechanisms are further needed to investigate the effects of those receptors and the downstream events.

A latest gene expression study on primary OPCs tissue culture provided by Dr. Cheng-ren Li also revealed a high expression of GalRs in OPCs with an undetectable level of GAL. In addition, the GalR2 expressed at a much higher level than did GalR1 (preliminary data, not shown in this thesis). This may further indicate that myelinating cell is not the source of GAL but the target of this peptide.

6.2. Summary

In summary, in the present study, we show that the breakdown of myelin due to CPZ-induced demyelination and promote re-myelination during the recovery phase was alleviated in Tg mice. Furthermore, we also found that the attenuated demyelination related impairments from the effect of elevated GAL resulted in the following: (1)

reduced death of mature oligodendrocytes, (2) suppressed proliferation of OPCs, and (3) restricted reactive astrogliosis. In addition, gene expression analysis revealed the differential responses of GalR1 and GalR2 in terms of demyelination and re-myelination. These findings strongly support the hypothesis that elevated circulating GAL levels alleviate CPZ-induced demyelination via GalR1. In this project, we also revealed that the administration of estrogen enhanced the protective effect of GAL on myelin, and the potential neuroprotective pathway of estrogen was considered to act via the stimulation of GAL. Demyelination is the last pathological downstream event of MS, and it is the core reason for the diverse symptoms and the ultimate disability caused by the disease. Meanwhile, re-myelination is the only hope for recovery for the MS patient. As the result of decades of study and practice, many achievements have been made in the development of treatments for the immuno-regulation for MS. However, the strategies of myelin protection and regeneration have been considered to be the next generation of therapy. Overall, our findings suggest a potential therapeutic effect for GAL on myelin protection and regeneration in MS, and may introduce next generation strategies for the treatment of MS.

CHAPTER 7: REFERENCES

Atlas of MS Database. Multiple Sclerosis International Federation. 2006 http://www.atlasofms.org/index.aspx

National Institutes of Health (NIH), Tutorials and Examples, http://imagej.nih.gov/ij/docs/examples/index.html

Allen, N.J., Barres, B.A., 2009. Neuroscience: Glia - more than just brain glue. Nature 457(7230), 675-677.

Aponso, P.M., Faull, R.L., Connor, B., 2008. Increased progenitor cell proliferation and astrogenesis in the partial progressive 6-hydroxydopamine model of Parkinson's disease. Neuroscience 151(4), 1142-1153.

Ascenzi, P., Bocedi, A., Marino, M., 2006. Structure-function relationship of estrogen receptor alpha and beta: impact on human health. Mol Aspects Med 27(4), 299-402.

Azevedo, F.A., Carvalho, L.R., Grinberg, L.T., Farfel, J.M., Ferretti, R.E., Leite, R.E., Jacob Filho, W., Lent, R., Herculano-Houzel, S., 2009. Equal numbers of neuronal and nonneuronal cells make the human brain an isometrically scaled-up primate brain. J Comp Neurol 513(5), 532-541.

Bacon, A., Holmes, F.E., Small, C.J., Ghatei, M., Mahoney, S., Bloom, S., Wynick, D., 2002. Transgenic over-expression of galanin in injured primary sensory neurons. Neuroreport 13(16), 2129-2132.

Barbarese, E., Carson, J.H., Braun, P.E., 1978. Accumulation of the four myelin basic proteins in mouse brain during development. J Neurochem 31(4), 779-782.

Barres, B.A., Raff, M.C., 1999. Axonal control of oligodendrocyte development. J Cell Biol 147(6), 1123-1128.

Bartfai, T., Hokfelt, T., Langel, U., 1993. Galanin--a neuroendocrine peptide. Crit Rev Neurobiol 7(3-4), 229-274.

Bartfai, T., Lu, X., Badie-Mahdavi, H., Barr, A.M., Mazarati, A., Hua, X.Y., Yaksh, T., Haberhauer, G., Ceide, S.C., Trembleau, L., Somogyi, L., Krock, L., Rebek, J., Jr., 2004. Galmic, a nonpeptide galanin receptor agonist, affects behaviors in seizure, pain, and forced-swim tests. Proc Natl Acad Sci U S A 101(28), 10470-10475.

Beal, M.F., MacGarvey, U., Swartz, K.J., 1990. Galanin immunoreactivity is increased in the nucleus basalis of Meynert in Alzheimer's disease. Ann Neurol 28(2), 157-161.

Bjartmar, C., Trapp, B.D., 2001. Axonal and neuronal degeneration in multiple sclerosis: mechanisms and functional consequences. Curr Opin Neurol 14(3), 271-278.

Branchek, T.A., Smith, K.E., Gerald, C., Walker, M.W., 2000. Galanin receptor subtypes. Trends Pharmacol Sci 21(3), 109-117.

Brodal, P., 2010. The central nervous system : structure and function, 4th ed. Oxford University Press, New York.

Buck, D., Hemmer, B., 2011. Treatment of multiple sclerosis: current concepts and future perspectives. J Neurol.

Campagnoni, C.W., Carey, G.D., Campagnoni, A.T., 1978. Synthesis of myelin basic proteins in the developing mouse brain. Arch Biochem Biophys 190(1), 118-125.

Chang, A., Nishiyama, A., Peterson, J., Prineas, J., Trapp, B.D., 2000. NG2-positive oligodendrocyte progenitor cells in adult human brain and multiple sclerosis lesions. J Neurosci 20(17), 6404-6412.

Chekhonin, V.P., Gurina, O.I., Dmitrieva, T.B., Semenova, A.V., Savchenko, E.A., Grigor'ev, M.E., 2000. [Myelin basic protein. Structure, properties, function and role in diagnosing demyelinating diseases]. Vopr Med Khim 46(6), 549-563.

Coelingh Bennink, H.J., 2004. Are all estrogens the same? Maturitas 47(4), 269-275.

Crawford, D.K., Mangiardi, M., Song, B., Patel, R., Du, S., Sofroniew, M.V., Voskuhl, R.R., Tiwari-Woodruff, S.K., 2010. Oestrogen receptor beta ligand: a novel treatment to enhance endogenous functional remyelination. Brain 133(10), 2999-3016.

Crawley, J.N., Mufson, E.J., Hohmann, J.G., Teklemichael, D., Steiner, R.A., Holmberg, K., Xu, Z.Q., Blakeman, K.H., Xu, X.J., Wiesenfeld-Hallin, Z., Bartfai, T., Hokfelt, T., 2002. Galanin overexpressing transgenic mice. Neuropeptides 36(2-3), 145-156.

Csepany, T., 2011. [Current treatment of multiple sclerosis]. Lege Artis Med 21(2), 97-104.

Davies, D., 2004. Child development : a practitioner's guide, 2nd ed. Guilford Press, New York.

Ding, X., MacTavish, D., Kar, S., Jhamandas, J.H., 2006. Galanin attenuates beta-amyloid (Abeta) toxicity in rat cholinergic basal forebrain neurons. Neurobiol Dis 21(2), 413-420.

Elliott-Hunt, C.R., Marsh, B., Bacon, A., Pope, R., Vanderplank, P., Wynick, D., 2004. Galanin acts as a neuroprotective factor to the hippocampus. Proc Natl Acad Sci U S A 101(14), 5105-5110.

Elliott-Hunt, C.R., Pope, R.J., Vanderplank, P., Wynick, D., 2007. Activation of the galanin receptor 2 (GalR2) protects the hippocampus from neuronal damage. J Neurochem 100(3), 780-789.

Ellison, J.A., de Vellis, J., 1994. Platelet-derived growth factor receptor is expressed by cells in the early oligodendrocyte lineage. J Neurosci Res 37(1), 116-128.

Evans, H., Baumgartner, M., Shine, J., Herzog, H., 1993. Genomic organization and localization of the gene encoding human preprogalanin. Genomics 18(3), 473-477.

Groebe, A., Clarner, T., Baumgartner, W., Dang, J., Beyer, C., Kipp, M., 2009. Cuprizone treatment induces distinct demyelination, astrocytosis, and microglia cell invasion or proliferation in the mouse cerebellum. Cerebellum 8(3), 163-174.

Hiller-Sturmhofel, S., Bartke, A., 1998. The endocrine system: an overview. Alcohol Health Res World 22(3), 153-164.

Hobson, S.A., Bacon, A., Elliot-Hunt, C.R., Holmes, F.E., Kerr, N.C., Pope, R., Vanderplank, P., Wynick, D., 2008. Galanin acts as a trophic factor to the central and peripheral nervous systems. Cell Mol Life Sci 65(12), 1806-1812.

Hokfelt, T., Broberger, C., Xu, Z.Q., Sergeyev, V., Ubink, R., Diez, M., 2000. Neuropeptides--an overview. Neuropharmacology 39(8), 1337-1356.

Hokfelt, T., Wiesenfeld-Hallin, Z., Villar, M., Melander, T., 1987. Increase of galanin-like immunoreactivity in rat dorsal root ganglion cells after peripheral axotomy. Neurosci Lett 83(3), 217-220.

Holmes, F.E., Mahoney, S., King, V.R., Bacon, A., Kerr, N.C., Pachnis, V., Curtis, R., Priestley, J.V., Wynick, D., 2000. Targeted disruption of the galanin gene reduces the number of sensory neurons and their regenerative capacity. Proc Natl Acad Sci U S A 97(21), 11563-11568.

Houben, H., Denef, C., 1994. Bioactive peptides in anterior pituitary cells. Peptides 15(3), 547-582.

Hwang, I.K., Yoo, K.Y., Kim, D.S., Do, S.G., Oh, Y.S., Kang, T.C., Han, B.H., Kim, J.S., Won, M.H., 2004. Expression and changes of galanin in neurons and microglia in the hippocampus after transient forebrain ischemia in gerbils. Brain Res 1023(2), 193-199.

Jurevics, H., Hostettler, J., Muse, E.D., Sammond, D.W., Matsushima, G.K., Toews, A.D., Morell, P., 2001. Cerebroside synthesis as a measure of the rate of remyelination following cuprizone-induced demyelination in brain. J Neurochem 77(4), 1067-1076.

Kaplan, L.M., Spindel, E.R., Isselbacher, K.J., Chin, W.W., 1988. Tissue-specific expression of the rat galanin gene. Proc Natl Acad Sci U S A 85(4), 1065-1069.

Kipp, M., Clarner, T., Dang, J., Copray, S., Beyer, C., 2009. The cuprizone animal model: new insights into an old story. Acta Neuropathol 118(6), 723-736.

Lang, R., Gundlach, A.L., Kofler, B., 2007. The galanin peptide family: receptor pharmacology, pleiotropic biological actions, and implications in health and disease. Pharmacol Ther 115(2), 177-207.

Lassmann, H., 2008. Models of multiple sclerosis: new insights into pathophysiology and repair. Curr Opin Neurol 21(3), 242-247.

Lee, H.Y., Hwang, I.K., Kim, D.H., Kim, J.H., Kim, C.H., Lim, B.O., Kang, T.C., Bang, K.H., Seong, N.S., Lee, H.J., Kim, J.D., Won, M.H., 2005. Ischemia-related changes in galanin expression in the dentate hilar region after transient forebrain ischemia in gerbils. Exp Anim 54(1), 21-27.

Liu, H.B., Loo, K.K., Palaszynski, K., Ashouri, J., Lubahn, D.B., Voskuhl, R.R., 2003. Estrogen receptor alpha mediates estrogen's immune protection in autoimmune disease. J Immunol 171(12), 6936-6940.

Lu, X., Lundstrom, L., Langel, U., Bartfai, T., 2005. Galanin receptor ligands. Neuropeptides 39(3), 143-146.

Lublin, F.D., Reingold, S.C., 1996. Defining the clinical course of multiple sclerosis: results of an international survey. National Multiple Sclerosis Society (USA) Advisory Committee on Clinical Trials of New Agents in Multiple Sclerosis. Neurology 46(4), 907-911.

Mahoney, S.A., Hosking, R., Farrant, S., Holmes, F.E., Jacoby, A.S., Shine, J., Iismaa, T.P., Scott, M.K., Schmidt, R., Wynick, D., 2003. The second galanin receptor GalR2 plays a key role in neurite outgrowth from adult sensory neurons. J Neurosci 23(2), 416-421.

Matsushima, G.K., Morell, P., 2001. The neurotoxicant, cuprizone, as a model to study demyelination and remyelination in the central nervous system. Brain Pathol 11(1), 107-116.

Mazarati, A., Lu, X., Kilk, K., Langel, U., Wasterlain, C., Bartfai, T., 2004. Galanin type 2 receptors regulate neuronal survival, susceptibility to seizures and seizure-induced neurogenesis in the dentate gyrus. Eur J Neurosci 19(12), 3235-3244.

Mechenthaler, I., 2008. Galanin and the neuroendocrine axes. Cell Mol Life Sci 65(12), 1826-1835.

Meister, B., Villar, M.J., Ceccatelli, S., Hokfelt, T., 1990. Localization of chemical messengers in magnocellular neurons of the hypothalamic supraoptic and paraventricular nuclei: an immunohistochemical study using experimental manipulations. Neuroscience 37(3), 603-633.

Mennicken, F., Hoffert, C., Pelletier, M., Ahmad, S., O'Donnell, D., 2002. Restricted distribution of galanin receptor 3 (GalR3) mRNA in the adult rat central nervous system. J Chem Neuroanat 24(4), 257-268.

Merchenthaler, I., 1991. The hypophysiotropic galanin system of the rat brain. Neuroscience 44(3), 643-654.

Merchenthaler, I., Lopez, F.J., Negro-Vilar, A., 1993. Anatomy and physiology of central galanin-containing pathways. Prog Neurobiol 40(6), 711-769.

Miron, V.E., Kuhlmann, T., Antel, J.P., 2011. Cells of the oligodendroglial lineage, myelination, and remyelination. Biochim Biophys Acta 1812(2), 184-193.

Morell, P., Greenfield, S., Costantino-Ceccarini, E., Wisniewski, H., 1972. Changes in the protein composition of mouse brain myelin during development. J Neurochem 19(11), 2545-2554.

Navikas, V., Link, H., 1996. Review: cytokines and the pathogenesis of multiple sclerosis. J Neurosci Res 45(4), 322-333.

Nilesson, G., 1950. A New Colour Reaction on Copper and Certain Carbonyl Compounds. Acta Chemica Scandinavica.

Nishiyama, A., Lin, X.H., Giese, N., Heldin, C.H., Stallcup, W.B., 1996. Co-localization of NG2 proteoglycan and PDGF alpha-receptor on O2A progenitor cells in the developing rat brain. J Neurosci Res 43(3), 299-314.

Norton, W.T., Poduslo, S.E., 1973. Myelination in rat brain: changes in myelin composition during brain maturation. J Neurochem 21(4), 759-773.

Ohtaki, T., Kumano, S., Ishibashi, Y., Ogi, K., Matsui, H., Harada, M., Kitada, C., Kurokawa, T., Onda, H., Fujino, M., 1999. Isolation and cDNA cloning of a novel galanin-like peptide (GALP) from porcine hypothalamus. J Biol Chem 274(52), 37041-37045.

Olek, M.J., 2005. Multiple sclerosis : etiology, diagnosis, and new treatment strategies. Humana Press, Totowa, N.J.

Orton, S.M., Herrera, B.M., Yee, I.M., Valdar, W., Ramagopalan, S.V., Sadovnick, A.D., Ebers, G.C., 2006. Sex ratio of multiple sclerosis in Canada: a longitudinal study. Lancet Neurol 5(11), 932-936.

Palkovits, M., 1992. Peptidergic neurotransmitters in the endocrine hypothalamus. Ciba Found Symp 168, 3-10; discussion 10-15.

Pardridge, W.M., 1983. Neuropeptides and the blood-brain barrier. Annu Rev Physiol 45, 73-82.

Perumal, P., Vrontakis, M.E., 2003. Transgenic mice over-expressing galanin exhibit pituitary adenomas and increased secretion of galanin, prolactin and growth hormone. J Endocrinol 179(2), 145-154.

Piaton, G., Aigrot, M.S., Williams, A., Moyon, S., Tepavcevic, V., Moutkine, I., Gras, J., Matho, K.S., Schmitt, A., Soellner, H., Huber, A.B., Ravassard, P., Lubetzki, C., 2011. Class 3 semaphorins influence oligodendrocyte precursor recruitment and remyelination in adult central nervous system. Brain.

Planas, B., Kolb, P.E., Raskind, M.A., Miller, M.A., 1997. Nerve growth factor induces galanin gene expression in the rat basal forebrain: implications for the treatment of cholinergic dysfunction. J Comp Neurol 379(4), 563-570.

Poritsanos, N.J., Mizuno, T.M., Lautatzis, M.E., Vrontakis, M., 2009. Chronic increase of circulating galanin levels induces obesity and marked alterations in lipid metabolism similar to metabolic syndrome. Int J Obes (Lond) 33(12), 1381-1389.

Prineas, J.W., Barnard, R.O., Kwon, E.E., Sharer, L.R., Cho, E.S., 1993. Multiple sclerosis: remyelination of nascent lesions. Ann Neurol 33(2), 137-151.

Readhead, C., Hood, L., 1990. The dysmyelinating mouse mutations shiverer (shi) and myelin deficient (shimld). Behav Genet 20(2), 213-234.

Rivers, L.E., Young, K.M., Rizzi, M., Jamen, F., Psachoulia, K., Wade, A., Kessaris, N., Richardson, W.D., 2008. PDGFRA/NG2 glia generate myelinating oligodendrocytes and piriform projection neurons in adult mice. Nat Neurosci 11(12), 1392-1401.

Rodriguez Diaz, M.A., Candal, E., Santos-Duran, G.N., Adrio, F., Rodriguez-Moldes, I., 2011. Comparative analysis of Met-enkephalin, galanin and GABA immunoreactivity in the developing trout preoptic-hypophyseal system. Gen Comp Endocrinol 173(1), 148-158.

Rossi, D., Volterra, A., 2009. Astrocytic dysfunction: insights on the role in neurodegeneration. Brain Res Bull 80(4-5), 224-232.

Salvati, S., Attorri, L., Avellino, C., Di Biase, A., Sanchez, M., 2000. Diet, lipids and brain development. Dev Neurosci 22(5-6), 481-487.

Santic, R., Schmidhuber, S.M., Lang, R., Rauch, I., Voglas, E., Eberhard, N., Bauer, J.W., Brain, S.D., Kofler, B., 2007. Alarin is a vasoactive peptide. Proc Natl Acad Sci U S A 104(24), 10217-10222.

Shen, P.J., Yuan, C.G., Ma, J., Cheng, S., Yao, M., Turnley, A.M., Gundlach, A.L., 2005. Galanin in neuro(glio)genesis: expression of galanin and receptors by progenitor cells in vivo and in vitro and effects of galanin on neurosphere proliferation. Neuropeptides 39(3), 201-205.

Sicotte, N.L., Liva, S.M., Klutch, R., Pfeiffer, P., Bouvier, S., Odesa, S., Wu, T.C., Voskuhl, R.R., 2002. Treatment of multiple sclerosis with the pregnancy hormone estriol. Ann Neurol 52(4), 421-428.

Siegel, G.J., 2006. Basic neurochemistry : molecular, cellular, and medical aspects, 7th ed. Elsevier, Amsterdam ; Boston.

Simmons, D.R., Spike, R.C., Todd, A.J., 1995. Galanin is contained in GABAergic neurons in the rat spinal dorsal horn. Neurosci Lett 187(2), 119-122.

Simons, M., Trotter, J., 2007. Wrapping it up: the cell biology of myelination. Curr Opin Neurobiol 17(5), 533-540.

Stuve, O., Oksenberg, J., 1993. Multiple Sclerosis Overview.

Szymusiak, R., Gvilia, I., McGinty, D., 2007. Hypothalamic control of sleep. Sleep Med 8(4), 291-301.

Tansey, F.A., Cammer, W., 1991. A pi form of glutathione-S-transferase is a myelin- and oligodendrocyte-associated enzyme in mouse brain. J Neurochem 57(1), 95-102.

Tatemoto, K., Rokaeus, A., Jornvall, H., McDonald, T.J., Mutt, V., 1983. Galanin - a novel biologically active peptide from porcine intestine. FEBS Lett 164(1), 124-128.

Tiwari-Woodruff, S., Morales, L.B., Lee, R., Voskuhl, R.R., 2007. Differential neuroprotective and antiinflammatory effects of estrogen receptor (ER)alpha and ERbeta ligand treatment. Proc Natl Acad Sci U S A 104(37), 14813-14818.

Tiwari-Woodruff, S., Voskuhl, R.R., 2009. Neuroprotective and anti-inflammatory effects of estrogen receptor ligand treatment in mice. J Neurol Sci 286(1-2), 81-85.

Torkildsen, O., Brunborg, L.A., Myhr, K.M., Bo, L., 2008. The cuprizone model for demyelination. Acta Neurol Scand Suppl 188, 72-76.

Venturini, G., 1973. Enzymic activities and sodium, potassium and copper concentrations in mouse brain and liver after cuprizone treatment in vivo. J Neurochem 21(5), 1147-1151.

Verge, V.M., Richardson, P.M., Wiesenfeld-Hallin, Z., Hokfelt, T., 1995. Differential influence of nerve growth factor on neuropeptide expression in vivo: a novel role in peptide suppression in adult sensory neurons. J Neurosci 15(3 Pt 1), 2081-2096.

Villar, M.J., Cortes, R., Theodorsson, E., Wiesenfeld-Hallin, Z., Schalling, M., Fahrenkrug, J., Emson, P.C., Hokfelt, T., 1989. Neuropeptide expression in rat dorsal root ganglion cells and spinal cord after peripheral nerve injury with special reference to galanin. Neuroscience 33(3), 587-604.

Villar, M.J., Meister, B., Cortes, R., Schalling, M., Morris, M., Hokfelt, T., 1990. Neuropeptide gene expression in hypothalamic magnocellular neurons of normal and hypophysectomized rats: a combined immunohistochemical and in situ hybridization study. Neuroscience 36(1), 181-199.

Vrontakis, M.E., 2002. Galanin: a biologically active peptide. Curr Drug Targets CNS Neurol Disord 1(6), 531-541.

Vrontakis, M.E., Peden, L.M., Duckworth, M.L., Friesen, H.G., 1987. Isolation and characterization of a complementary DNA (galanin) clone from estrogen-induced pituitary tumor messenger RNA. J Biol Chem 262(35), 16755-16758.

Vrontakis, M.E., Yamamoto, T., Schroedter, I.C., Nagy, J.I., Friesen, H.G., 1989. Estrogen induction of galanin synthesis in the rat anterior pituitary gland demonstrated by in situ hybridization and immunohistochemistry. Neurosci Lett 100(1-3), 59-64.

Walton, K.M., Chin, J.E., Duplantier, A.J., Mather, R.J., 2006. Galanin function in the central nervous system. Curr Opin Drug Discov Devel 9(5), 560-570.

Werner, F.M., Covenas, R., 2010. Classical neurotransmitters and neuropeptides involved in major depression: a review. Int J Neurosci 120(7), 455-470.

Wiesenfeld-Hallin, Z., Xu, X.J., 1998. Galanin in somatosensory function. Ann N Y Acad Sci 863, 383-389.

Wolosker, H., Dumin, E., Balan, L., Foltyn, V.N., 2008. D-amino acids in the brain: D-serine in neurotransmission and neurodegeneration. FEBS J 275(14), 3514-3526.

Zatta, P., Raso, M., Zambenedetti, P., Wittkowski, W., Messori, L., Piccioli, F., Mauri, P.L., Beltramini, M., 2005. Copper and zinc dismetabolism in the mouse brain upon chronic cuprizone treatment. Cell Mol Life Sci 62(13), 1502-1513.

Zhang, J., Kramer, E.G., Mahase, S., Dutta, D.J., Bonnamain, V., Argaw, A.T., John, G.R., 2011. Targeting oligodendrocyte protection and remyelination in multiple sclerosis. Mt Sinai J Med 78(2), 244-257.

Zhang, Y., Xu, H., Jiang, W., Xiao, L., Yan, B., He, J., Wang, Y., Bi, X., Li, X., Kong, J., Li, X.M., 2008. Quetiapine alleviates the cuprizone-induced white matter pathology in the brain of C57BL/6 mouse. Schizophr Res 106(2-3), 182-191.